BAND-OFFSET RATIO CALCULATIONS OF NITROGEN CONTAINING III-V QUANTUM WELLS

M. Sc. Thesis

in

Engineering Physics
University of Gaziantep

by
Fatma KOÇAK
September 2003

Approval of the Graduate School of Natural and Applied Sciences

Prof. Dr. Bülent GÖNÜL
Director

I certify that this thesis satisfies all the requirements as a thesis for the degree of Master of Science.

Prof. Dr. Ömer F.BAKKALOĞLU
Head of Department

This is to certify that we have read this thesis and that in our opinion it is fully adequate, in scope and quality, as a thesis for the degree of Master of Science.

Assoc. Prof. Dr. Beşire GÖNÜL
Supervisor

Examining Committee Members

Assoc. Prof. Dr. Beşire GÖNÜL
.....

Assist. Prof. Dr. Necmettin YAZICI
.....

Assist. Prof. Dr. Mustafa ÖZTAŞ
.....

ABSTRACT

BAND-OFFSET RATIO CALCULATIONS OF NITROGEN CONTAINING III-V QUANTUM WELLS

KOÇAK, Fatma
M. Sc., Engineering Physics Department
Supervisor: Assoc. Prof. Dr. Beşire GÖNÜL
September 2003, 58 Pages

A comparative study of the band-offset ratio of the three competing laser materials, namely InGaAsP-InP, AlGaInAs-InP, and GaInNAs-GaAs has been undertaken. Our theoretical study shows that model solid theory can be used to calculate the band offset ratios of the GaInNAs-GaAs for small nitrogen concentration including the effect of strain and modifications in conduction band but neglecting the direct effect of nitrogen. We have calculated that the alternative AlGaInAs and GaInNAs laser systems have substantially better band alignment than the commonly used InGaAsP. Strain compensation brings further benefits to that of the three competing laser systems. Therefore, high temperature operation has been anticipated in these alternative material systems with strain compensated barriers due to better electron and hole confinement as a result of the increased band offset and a more favourable band offset ratio. Our theoretical calculations indicate a significant increase in conduction band offset ratio and a decrease in valence band offset ratio with the introduction of nitrogen to InGaAs. This result highlights the intrinsic superiority of the N-based laser system.

Keywords: III-V Semiconductors, Nitrides, Quantum Well Lasers, Band-offset ratios, Band alignments.

ÖZET

NİTROJEN İÇEREN III-V KUVANTUM KUYULARININ BANT-DERİNLİK ORANININ HESAPLANMASI

KOÇAK, Fatma
Yüksek Lisans Tezi
Fizik Mühendisliği Bölümü
Tez Danışmanı: Doç. Dr. Beşire GÖNÜL
Eylül 2003, 58 sayfa

Bu tezde üç farklı yapıdaki lazer malzemesi (InGaAsP-InP, AlGaInAs-InP, ve GaInNAs-GaAs)'nin bant derinlik oranları hesaplandı ve karşılaştırması yapıldı. Teorik çalışmamız gösterdi ki Model Solid Teoriyi GaInNAs' ın küçük nitrojen yoğunluğuna sahip olduğunda ve örgünün orijinal uzunluktaki değişiminin etkisi (strain) ile iletim bandındaki değişiklikleri içerip nitrojenin doğrudan etkisini ihmal ettiğimizde bant derinliğini hesaplamada kullanabiliriz. Ayrıca bu çalışmada yoğun olarak kullanılan InGaAsP den çok daha iyi bant dizilişine sahip alternatif lazer sistemlerini de hesapladık. Örgü sabitleri farklı olan tabakalar birbiri üzerine büyütüldüğünde orijinal örgü sabitinde germe ve sıkıştırma olmak üzere iki tür değişiklik oluşur ve buna orijinal uzunluğuna nazaran oluşan değişim (strain) denir. Kuyudaki değişim engele uygulanan değişimle nötürleştirilebilir (strain compensation), bu nötürleştirme işleminin yukarıda bahsettiğimiz üç lazer sisteme oldukça büyük fayda sağladığı çalışmalardan anlaşılmıştır. Bu işlem neticesinde bant derinliği arttığından elektron ve boşlukların daha iyi hapsolunması sağlanır, bu ise yüksek ısı işlemlerinde istenilen bir durumdur. Teorik hesaplamalarımız InGaAs'a nitrojen katmakla iletim bant derinlik oranında önemli bir artış ve yalıtım bant oranında da önemli bir azalma olduğunu göstermiştir. Bu sonuç nitrojen temelli lazer sistemlerine dikkate değer bir üstünlük sağlamaktadır.

Anahtar Kelimeler: III-V Yarıiletkenleri, nitrit, kuantum kuyu lazerleri, bant derinlik oranı, bant dizilişi

ACKNOWLEDGEMENT

The author would like to express sincere appreciation to her supervisor Assoc. Prof. Dr. Beşire GÖNÜL for her guidance and helpful discussions. Her encouragement and valuable suggestions caused to construct this thesis.

Author's special thanks go to her husband Mehmet KOÇAK for his continuous support to construct this thesis in every steps.

She dedicate this work to her family especially for her daughter Nursena KOÇAK.

TABLE OF CONTENTS

ABSTRACT.....iii

ÖZET.....iv

ACKNOWLEDGEMENT.....v

TABLE OF CONTENTS.....vi

LIST OF FIGURES.....viii

LIST OF TABLES.....xi

1. INTRODUCTION.....1

2. HETEROJUNCTION LASERS.....6

2.1. Single Heterostructure.....7

2.1.1. Isotype.....7

2.1.2. Anisotype.....9

2.2. Double Heterostructure.....10

2.3. Energy Band Parameters.....13

2.4. Band-Offsets.....15

2.5. Band Gap Against Stochiometry.....17

2.6. Summary.....18

3. MODEL BAND-OFFSET CALCULATIONS FOR III-V AND NITROGEN CONTAINING III-V SEMICONDUCTOR LASER MATERIAL SYSTEMS 19

3.1. Introduction 19

3.2. Calculation of Bulk Band Gap with Strain 20

3.3. Theoretical Models for the Calculation of Band-Offsets 23

3.3.1. Model Solid Theory 24

3.3.2. Harrison's model 25

3.4. Band-Anti-Crossing Model 26

3.5. Conclusions 27

4. THEORETICAL COMPARISON OF THE BAND-OFFSET RATIOS USING MODEL SOLID THEORY AND HARRISON'S MODEL 28

4.1. Introduction 28

4.2. Comparison of the Band Models for Phosphide system 28

4.3. Comparison of the Band Models for Aluminium system 33

4.4. Calculation of the Band Alignment of Nitrogen System by Means of Model Solid Theory 36

4.5. Conclusion 39

5. A THEORETICAL COMPARISON OF THE BAND-OFFSET RATIOS OF PHOSPHORUS-ALUMİNİUM-AND-NITROGEN BASED 1.3 μm QW LASERS 40

6. CONCLUSIONS 53

REFERENCES 54

PUBLICATIONS 58

LIST OF FIGURES

Figure 2.1 Isotype heterojunctions : (a) N and n separated, (b) band diagram through an N-n junction, (c) impossible alternative to (b), and (d) band diagram trough a P-p junction.

Figure 2.2 Band diagrams of anisotype heterojunctions: N-p (a) separated, and (b) joined; p-n (c) separated, and (d) joined.

Figure 2.3 A double heterojunction system: (a) structure of NpP, band diagram with (b) no bias, and (c) forward bias, (d) PnN system with no bias, (e) with bias, and (f) refractive index variation trough the junction.

Figure 2.4 Historical trend in threshold current density of early GaAs-based laser diodes.

Figure 2.5 A comparison of the threshold current density dependence on temperature for homojunction and heterojunction lasers.

Figure 2.6 Parameters used in the calculation of ΔE_C and ΔE_V in a heterojunction.

Figure 2.7 Energy band line-up diagram for a quantum well structure. Conduction and valence band offsets are indicated.

Figure 4.1 The variation of conduction band-offset ΔE_C and valence band-offset ΔE_V versus P concentration and % strain in well according to (a) Model solid theory and (b) Harrison's model.

Figure 4.2 The variation of conduction band-offset ratio Q_C and valence band-offset ratio Q_V versus phosphorus P concentration and % strain in well according to (a) Model solid theory and (b) Harrison's model.

Figure 4.3 The variation of conduction band offset ΔE_C and valence band offset ΔE_V (a), and the variation of conduction band offset ratio Q_C and valence band offset ratio Q_V (b) versus P concentration and % strain in the barrier according to Harrison's model.

Figure 4.4 The variation of conduction band-offset ΔE_C and valence band-offset ΔE_V versus aluminium Al concentration and % strain in well according to (a) Model solid theory and (b) Harrison's model.

Figure 4.5 The variation of conduction band-offset ratio Q_C and valence band-offset ratio Q_V versus Al concentration and % strain in well according to (a) Model solid theory and (b) Harrison's model.

Figure 4.6 The variation of conduction band offset ΔE_C and valence band offset ΔE_V (a), and the variation of conduction band offset ratio Q_C and valence band offset ratio Q_V (b) versus Al concentration and % strain in the barrier according to Harrison's model.

Figure 4.7 Schematic diagram of the bulkbandgap of the GaInNAs alloy, according to the BAC model.

Figure 4.8 The variation of conduction band-offset ΔE_C and valence band-offset ΔE_V versus N concentration and % strain in the well according to Model solid theory.

Figure 4.9 The variation of conduction band-offset ratio Q_C and valence band-offset ratio Q_V versus N concentration and % strain in the well according to Model solid theory.

Figure 5.1 The phosphorus concentration (in well) dependence of the conduction and valence band offset ratios of the uncompensated $In_{0.83}Ga_{0.17}As_{1-y}P_y/In_{0.9}Ga_{0.1}As_{0.24}P_{0.76}$/InP laser system according to Harrison's model.

Figure 5.2 The variation of the conduction and valence band offsets with phosphorus concentration and compressive strain (in well) for uncompensated $In_{0.83}Ga_{0.17}As_{1-y}P_y/In_{0.9}Ga_{0.1}As_{0.24}P_{0.76}$/InP laser system according to Harrison's model.

Figure 5.3 The calculated variation of the conduction and valence band offsets with phosphorus concentration and tensile strain (in barrier) for compensated $In_{0.83}Ga_{0.17}As_{0.66}P_{0.34}/In_{0.9}Ga_{0.1}As_{1-y}P_y$ / InP laser system according to Harrison's model.

Figure 5.4 The aluminium concentration (in well) dependence of the conduction and valence band offset ratios of the uncompensated $Al_yGa_xIn_{1-x-y}As/Al_{0.37}Ga_{0.095}In_{0.535}As$/InP laser system according to Harrison's model; gallium content in the well is kept at 0.095.

Figure 5.5 The variation of the conduction and valence band offsets with aluminium concentration and compressive strain (in well) for uncompensated $Al_yGa_xIn_{1-x-y}As/Al_{0.37}Ga_{0.095}In_{0.535}As/InP$ lasers system according to Harrison's model; gallium content in the well is kept at 0.095.

Figure 5.6 The calculated variation of the conduction and valence band offsets with aluminium concentration and tensile strain (in barrier) for compensated $Al_{0.175}Ga_{0.095}In_{0.73}As/ Al_yGa_xIn_{1-x-y}As$ / InP laser system according to Harrison's model; x=0.095.

Figure 5.7 The nitrogen concentration (in well) dependence of the conduction and valence band offset ratios of the uncompensated $Ga_{0.9}In_{0.1}N_yAs_{1-y}/Al_{0.1}Ga_{0.9}As/GaAs$ laser system according to model solid theory.

Figure 5.8 The variation of the conduction and valence band offsets with nitrogen concentration and compressive strain (in well) for uncompensated $Ga_{0.9}In_{0.1}N_yAs_{1-y}/Al_{0.1}Ga_{0.9}As/GaAs$ laser system according to model solid theory.

Figure 5.9 The variation of the conduction and valence band offset ratios with phosphorus concentration and tensile strain (in barrier) for compensated $Ga_{0.9}In_{0.1}N_{0.025}As_{0.975}/GaAs_{1-y}P_y/GaAs$ laser system according to model solid theory.

Figure 5.10 The calculated variation of the conduction and valence band offsets with phosphorus concentration and tensile strain (in barrier) for compensated $Ga_{0.9}In_{0.1}N_{0.025}As_{0.975}/GaAs_{1-y}P_y/GaAs$ laser system according to model solid theory.

LIST OF TABLES

Table 2.1 Values of band gap E_g and electron affinity χ for various semiconductors.

Table 2.2 Values of the c parameter for various semiconductors.

Table 3.1 Material parameters for the calculation for InGaAsP, AlGaInAs and GaInNAs material systems.

Table 3.2 Parameters for the calculation of band alignment of the $In_{1-x}Ga_xAs_yP_{1-y}$, $In_{1-x-y}Ga_xAl_y As$ and $Ga_xIn_{1-x}N_yAs_{1-y}$ material systems.

CHAPTER 1

INTRODUCTION

Long wavelength quantum-well (QW) lasers based upon InGaAsP materials are widely used in optical communications applications, but the temperature dependence of these lasers remains an issue that limits their performance at high temperature. This results in the need for cooling units that increase the cost of the packaged lasers and the overall power consumption of the device as well as reducing device reliability. Impaired high-temperature performance is thought to arise due to reduced electron confinement and increased Auger losses [1-3]. Thus, in recent years, different material systems have been sought to improve the active region performance, including AlGaInAs and InGaAsN. High-temperature operation has been anticipated in these material systems due to better electron and hole confinement as a result of increased band offsets and a more favourable band-offset ratio [4,5]. An additional advantage of InGaAsN is that it is lattice matched to GaAs, enabling integrated growth of AlAs-GaAs distributed Bragg reflectors (DBRs) for vertical-cavity surface-emitting lasers (VCSELs). This also enables large-scale fabrication on larger GaAs substrates [5].

It has been shown that band gap offset engineering can significantly improve the performance of electronic devices and photonic devices [6]. In general band gap offset engineering includes the choice of semiconductor material to form the optimized heterojunction and artificially modifying the band gap offset. It has been stated that [6], in addition to strain, optimization of the band gap offset

also leads to improved performance in quantum well lasers, especially in enabling a simultaneous attainment of ultralow threshold current. The improvement stems from optimizing the band gap offset at the QW heterojuncions since the asymmetry between the conduction band (CB) and the valence band (VB) structures in the optical confining region is compensated by the corresponding optimal band gap offset at the QW. In this thesis, we show theoretically how the band gap offset at QW heterojunctions can be optimized by means of using different semiconductor materials as laser materials and different laser designs. The results provide general guidelines to the design of high performance of QW lasers as well as suggest applications to other active laser devices.

Since density of states of a two-dimensional electron gas near the energy gap is larger than that of a bulk material, single quantum well (SQW) lasers have a higher material gain than bulk active region lasers [7]. However, the optical occupation factor of a quantum well is very small and so is the modal gain. In order to achieve high quantum efficiency and low threshold current density, SQW lasers should have large cavity length and small free carrier absorption in the waveguide layer. Quantum-well lasers have been successfully demonstrated for a GaAlAs-GaAs material system [8,9] and have become an industrial reality. GaAlAs-GaAs lasers with one or two 40Å – 100Å wide quantum wells have been adopted for most practical applications [10]. In the latter material system the discontinuities of conduction bands are larger than those of valence bands. Therefore quantization of both electron and hole states in quantum wells is possible in spite of a small ratio of electron and holes effective masses. Large differences in energy gaps and refractive indices between GaAs and AlAs allow both the electronic properties mentioned above and a high value of the optical occupation factor.

It is difficult to obtain similar conditions for an InGaAsP-InP system used for communication lasers due to a small conduction band discontinuity between InP and the active region material [11]. In addition, a low potential barrier for electrons between the active and cladding regions also results in thermionic emission of electrons out of the active layer [12,13]. In order to overcome this problem, a high doping level of cladding layers is necessary, producing high optical absorption of the lasing mode. An adequate modal gain for this type of laser has been achieved by stacking quantum wells and separating them with potential barriers, thus forming a multi-quantum-well (MQW) structure, However due to the noted problems and

Auger recombination characterizing narrow-gap materials, InGaAsP-InP-based lasers demonstrate strong temperature dependence on threshold currents and external quantum efficiency [14].

An improved temperature performance of 1.3μm strained quantum-well lasers was reported in [15], where InGaAlAs-InP material system was used to increase the electron confinement energy. The result was attainable due to a better fit of the discontinuities of the conduction and valence bands of AlInAs and GaInAs (matching those of InP). The characteristic temperature of threshold current (T_0) reported in [15] was 80 K.

In recent past years, quantum-well (QW) laser diodes of diluted nitrides, GaInNAs, grown on GaAs substrates have emerged as viable alternatives to the dominating InP-based heterostructure lasers currently being used in silica optical fibre communications [16] at the 1.3μm transmission window. Adding nitrogen, in a dilute concentration regime, to InGaAs produces a drastic decrease of the fundamental band gap of the material [17] facilitating light sources that operate at wavelengths beyond the usual spectral range of GaAs-based semiconductors. At the same time, band offsets for a GaInNAs/GaAs QW are larger than those for a conventional GaInAsP/InP QW, providing enhanced confinement for charge carriers and thus excellent high-temperature characteristics [5,18]. An N-related increase in localization character of the lowest confined electron level and hence, an increase of its temperature insensitivity also beneficially contributes to laser temperature performances [19,20]. Another beneficial feature of GaInNAs, in addition to a longer wavelength attainable and a possibility of using a low-cost GaAs substrate, is the fact that the effective mass of the conduction band edge is increased compared to that of GaInAs, providing a closer match between the effective masses of electrons and holes [21].

Long-wavelength (1.3μm) active regions grown on GaAs substrates have potential for temperature-insensitive performance due to the larger bandgap discontinuities than found in conventional InP-based structures. Several approaches have been used to achieve long-wavelength emission on GaAs substrates, ranging from the use of InGaAs quantum dots (QD's), highly strained quantum InGaAs wells (QW's) and InGaAsN QW s.

Strained-layer quantum well structures have been widely used for optoelectronic devices. In particular, quantum well laser diodes emitting at wavelengths of 0.98 and 1.5μm have exhibited excellent characteristics if their quantum wells are under lattice strain [22,23]. As the number of strained quantum wells is increased, the total strain in the structure accumulates and the total strained-layer thickness approaches a critical layer thickness at which lattice misfit dislocations start to form. Therefore, the incorporation of strain limits the number of quantum wells that may be used without inducing an unacceptably high density of misfit dislocations. For many devices, such as lasers and optical modulators, a large number of quantum well is required for optimal performance. Strain –compensation techniques prevent the formation of dislocations by alternating layers with compressive and tensile-strain of equal amounts, resulting in zero net strain. In lasers that require high gain and thus many QW' s, e.g., vertical-cavity surface emitting lasers (VCSEL' s), strain compensation may be used to increase the number of compressively strained wells without inducing defects. Therefore, there has been interest in strain-compensated quantum well structures where the barrier layers are under tensile strain and quantum wells are under compressive strain. The strain-thickness product of barriers can be made equal in magnitude, but opposite in sign to that of wells to yield a multiple-quantum well (MQW) stack with zero net strain.

Semiconductor lasers emitting near 1μm wavelength fabricated using InGaAs-GaAs material system have been widely studied. The light emitting InGaAs region in this laser is sandwiched between AlGaAs or InGaP layers, which are further, sandwiched between AlGaAs or InGaP layers, which are lattice, matched to GaAs. For emission wavelength near 1μm, the composition of the light emitting region is typically $In_{0.2}Ga_{0.8}As$ [24,25]. For this composition, the lattice constant of $In_{0.2}Ga_{0.8}As$ is about 1.5% larger than that for GaAs. This results in a compressively strained active region for the InGaAs-GaAs laser emitting near 1μm. Recently, a strain compensated laser structure emitting near 1μm has been reported [26]. In this laser structure, the $In_{0.2}Ga_{0.8}As$ active region is sandwiched between $GaAs_{0.8}P_{0.2}$ layers. The lattice constant of $GaAs_{0.8}P_{0.2}$ is about 0.8% smaller than that of GaAs. Thus by forming a multi-quantum well active region with $In_{0.2}Ga_{0.8}As$ quantum well light emitting region (N_a layers of thickness t_a) and $GaAs_{0.8}P_{0.2}$ barrier layers (N_b layers of thickness t_b) such that $N_a t_a \delta_a + N_a t_b \delta_b \cong 0$, it is possible to have a closely

strain compensated or partially strain compensated active region. The quantities δ_a, δ_b in the above equation are the lattice constant differences between the active region and GaAs and barrier region and GaAs, respectively. Since δ_a and δ_b are of opposite sign, it is possible to satisfy the above equation by choosing proper t_a and t_b for given values of δ_a and δ_b. The light emitting layers in the strain compensated multi-quantum-well (MQW) laser are effectively under a larger amount of compressive stress than that for a regular strained MQW laser. This effect results in larger gain coefficient and smaller linewidth enhancement factor for strained compensated lasers relative to conventional factor for strained layer lasers.

CHAPTER 2

HETEROJUNCTION LASERS

Early semiconductor lasers based on homojunctions were little more than laboratory curiosities, used largely to look at the basic physics of stimulated emission and gain, rather than with any technological application in mind. They were inferior to other lasers in many respects, namely:

(i) they could only operate at low temperature, usually in pulsed mode with high drive currents (~10^5 Acm^{-2})-room temperature generation demanding even higher current operation (~10^5 Acm^{-2}),

(ii) the output had a large spectral width compared to other lasers sources, especially gas lasers,

(iii) the output was not spatially coherent, because of diffraction at the output aperture,

(iv) output power was very low in comparison with other lasers,

(v) reliability was poor, with devices showing a rapid decay in performance and premature failure.

Devices were made in most III-V materials as well as many other compound semiconductors, and given in [27] is a complete list of homojunction materials that exhibit laser action, including excitation mechanism .

The proposal for using optical fibers as media for light wave communications revived the interest in semiconductor lasers from a technology point of view. Here was a real use for such a laser, where the small size of the device and its power supply were its major advantages over other lasers. The timing of this proposal coincided with the maturing of both crystal growth and several of the epitaxial

technologies needed for heterostructure devices. There was suddenly a demand to solve the problem of reliability, room temperature operation and threshold current, along with the technologies potentially able to solve these problems. It wasn't long before heterostructure lasers were being made, and then double heterostructure devices, and soon an initially bewildering range of device designs to overcome different aspects of laser operation were being published; new structures are being proposed and made even now, showing that the scope for innovation is far from limited.

This chapter reviews the basic heterostructure device, and how its performance is an improvement over a homojunction system. Double heterostructures are then introduced, a review of the semiconductor material used is presented, and then a selection of the significant designs are discussed.

2.1 Single Heterostructure

The problems with a homojunction device which can be overcome with a heterostructure are:

(i) poor optical confinement,
(ii) marginal population inversion,
(iii) poor carrier confinement,

all three of which lead to a high operating current, which is a major factor in device degradation and hence long term reliability. To overcome the above problems that it was meet in a homojunction device, the heterostructure can be offered as a solution. It is then worthwhile to briefly review here the working of the two types of heterostructure, isotype (N-n or P-p) and anisotype (N-p or P-n), where the capital letter signifies the material of higher bandgap.

2.1.1 Isotype

Examples of both N-n and P-p isotype heterojunctions are shown in figures 2.1 (b) and (d) respectively. In fig. 2.1 (b) the conduction band on the N side bends upwards, whilst on the n-side it bends downwards. At first this behaviour might seen

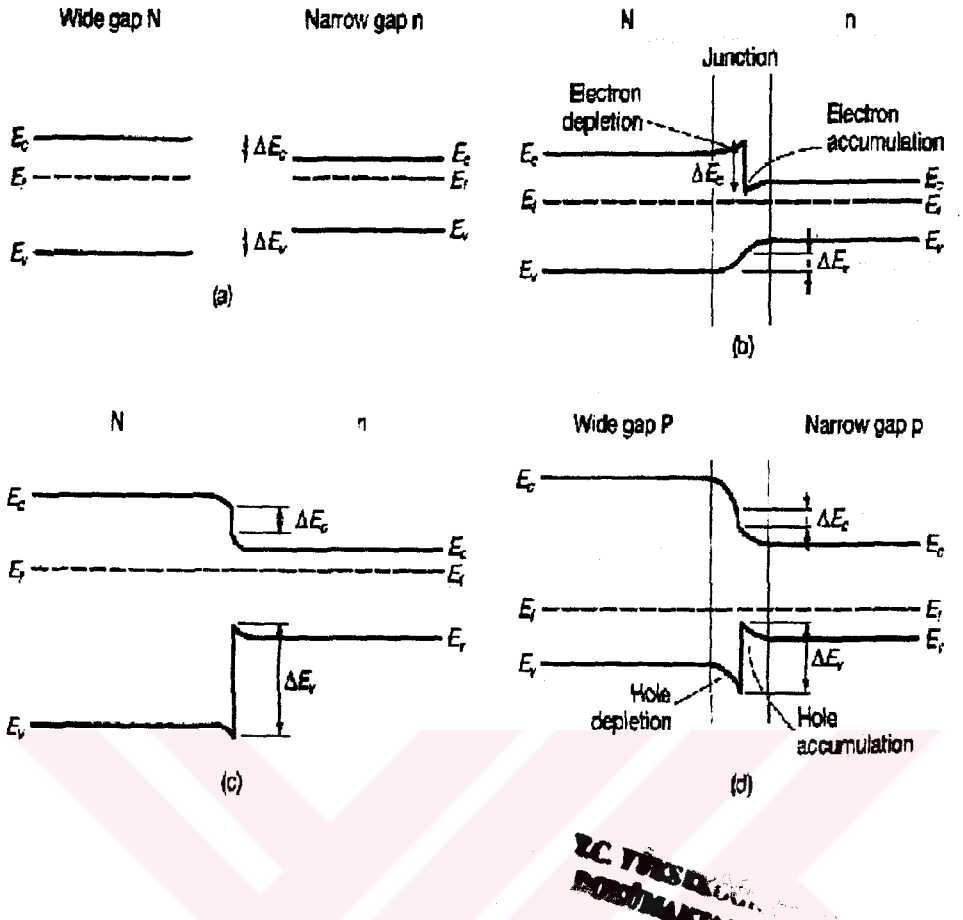

Figure 2.1 Isotype heterojunctions : (a) N and n separated, (b) band diagram through an N-n junction, (c) impossible alternative to (b), and (d) band diagram trough a P-p junction [28].

confusing, especially as the valence band only has a small discontinuity. But if we remember that for any junction in equilibrium (i) the Fermi levels must be equal, and (ii) the band gap in any semiconductor must be constant within that material (for a given doping) then the situation becomes clearer. For N and n separated, as in fig. 2.1(a), there will be a difference in conduction band and valence band energies, relative to a constant Fermi level, of ΔE_C and ΔE_V respectively. Thus bringing N and n together results in E_V bending up on the N-side and down on the n-side, with E_C correspondingly moving up or down on the N-or n-side respectively to maintain the band gap. At the junction there will be discontinuities in both E_V and E_C. As seen from fig. 2.1(a), in going from N to n, ΔE_V is positive. So there will be a positive discontinuity in E_V after junction formation given by ΔE_V. Similarly, the negative value of ΔE_C in fig. 2.1(a) gives a negative discontinuity in E_C after junction

formation; however, here the two conduction bands are moving in opposite directions, and hence ΔE_C appears as a spike. Hence, as shown in fig. 2.1(b), the rise in E_C on the N-side acts to deplete this region of electrons, whilst the fall in E_C on the n-side acts as an accumulation, electron confinement region.

At first, a plausible alternative to the diagram of fig. 2.1(b) might seem possible. Why is the spike in E_C, and not E_V in other words, isn't the band diagram of fig. 2.1(c) equally possible? A further consideration of junction formation will see why this is not so. In forming the junction, the electrons flow from a high potential region to a low potential region until the Fermi levels have equalized, in our case from N to n. This leads to depletion on the N-side and accumulation on the n-side, given the corresponding band bending as in fig. 2.1(b). The formation of a potential barrier ΔE_C at equilibrium prevents further electron movement. In fig. 2.1(c), there is no barrier in E_C to charge movement, implying that electrons are free to move indefinitely. Clearly this is untrue, and so fig. 2.1(c) cannot represent an energy model of carrier movements; fig. 2.1(b) is then the correct interpretation.

A band structure for a P-p contact is shown in fig. 2.1(d). Similarly to the N-n contact, hole transfer from P to p cause a hole potential barrier at the interface, and hence corresponding depletion and accumulation layers. ΔE_C and ΔE_V also appear, and are similarly defined as for the N-n structure.

2.1.2 Anisotype

Equilibrium band diagrams for N-p and P-n contacts are shown in fig. 2.2. A spike appears both in the conduction band on the N-p system (fig. 2.2(b)) and in the valence band of the P-n system (fig. 2.2(d)). Majority carriers are thus held back from moving from the wide gap material to the narrow gap. Similarly majority carriers are held in the narrow gap material by the large difference in either E_V (N-p junction) or E_C (P-n junction).

Single heterostructure (SH) lasers did alleviate the problems mentioned at the beginning of this section, but their practical use was short lived as it became clear that double heterostructure (DH) lasers were needed, and these were produced within a year of the first SH laser.

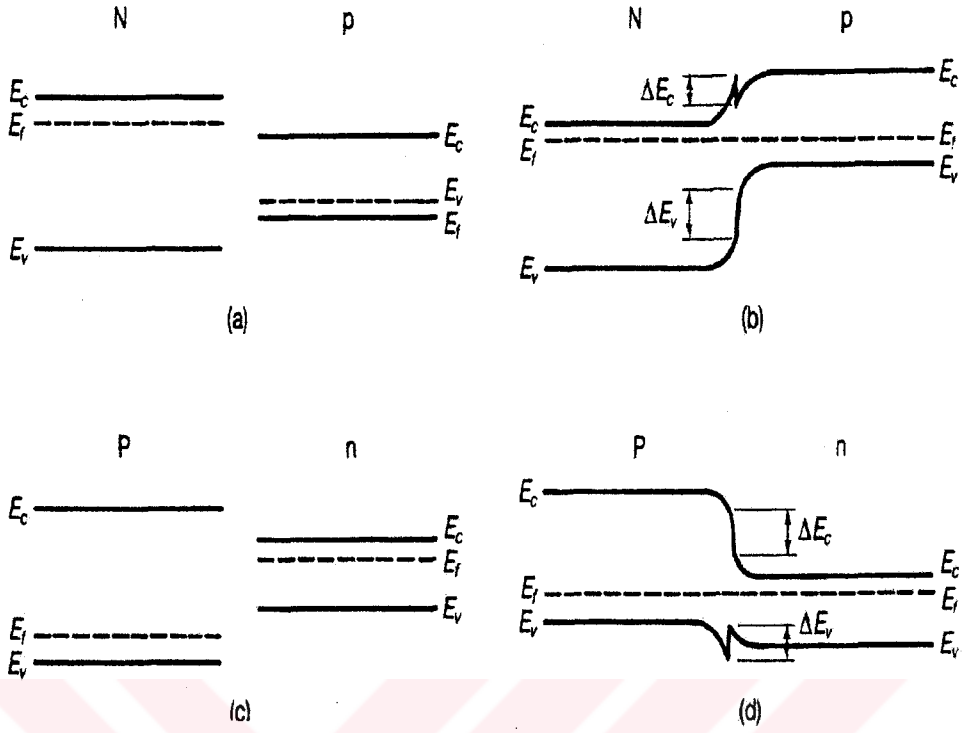

Figure 2.2 Band diagrams of anisotype heterojunctions: N-p (a) separated, and (b) joined; p-n (c) separated, and (d) joined [28].

2.2 Double Heterostructure

The advantages of a DH laser over both a single heterostructure and especially a homojunction system will be apparent from a discussion of fig. 2.3. This shows a double heterostructure system consisting of one isotype (p-GaAs to P-AlGaAs) and one anisotype (p-GaAs to N-AlGaAs) junction (fig. 2.3(a)). Extracting the relevant combinations from figures 2.1 and 2.2 the equilibrium band diagram through movement from N to p given by the spike in E_C, and from p to P given by the large potential barrier at this interface. There are similar restrictions on hole movement at the two interfaces. With the application of sufficient forward bias (see fig. 2.3(c)) some electrons have enough energy to overcome the N-p spike in E_C and enter the p-doped central region. However, they are still prevented from leaving at the p-P junction because the barrier there is still large. Thus a large number of injected carriers are confined more readily,

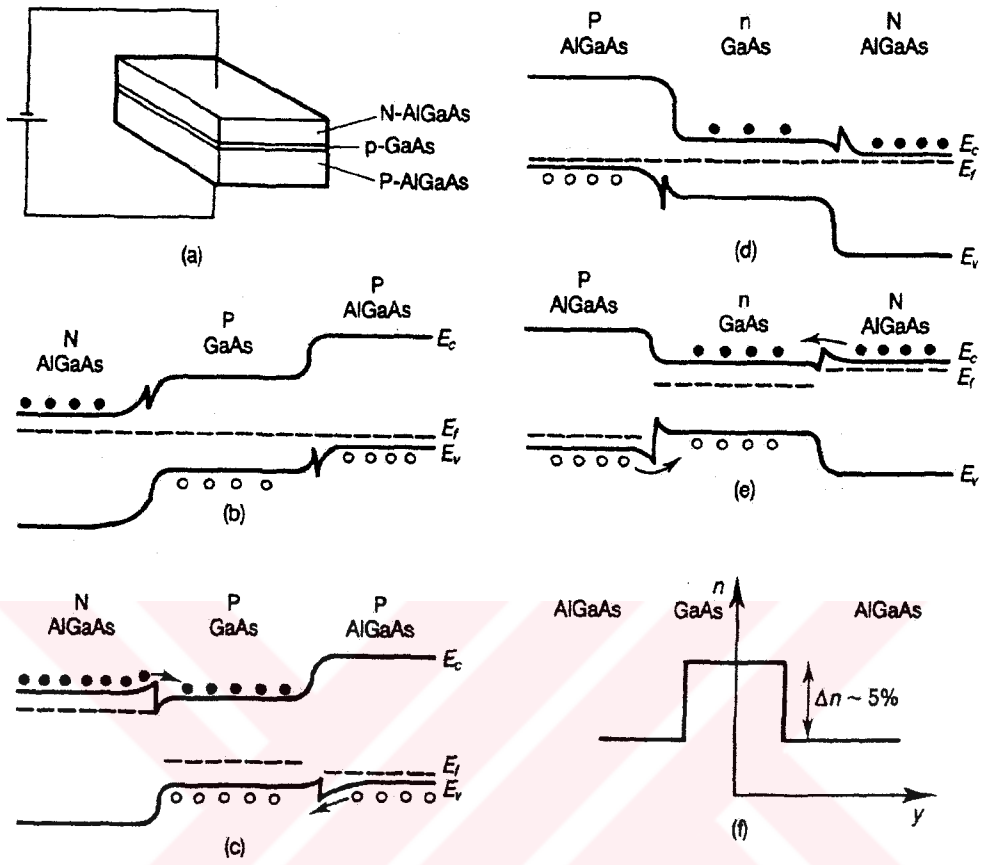

Figure 2.3 A double heterojunction system: (a) structure of NpP, band diagram with (b) no bias, and (c) forward bias, (d) PnN system with no bias, (e) with bias, and (f) refractive index variation trough the junction [28].

obtaining a population inversion with a lower threshold current. A similar diagram can be drawn for a PnN system under both equilibrium and forward bias conditions (figures 2.3(d) and (e)). Here we have degenerate n-type region as the central layer, and the injection of holes from P to n in forward bias creates the population inversion.

For both NpP or PnN structures there are two further advantages of DH systems: the sandwich formed by two wide gap materials either side of a narrow gap material leads to a large refractive index difference. The refractive index difference between the population inversion region and the surrounding semiconductor is brought about by the high carrier densities, and it is of the order of 0.1- 1.0 %. For

heterostructure systems, wide gap materials have a smaller refractive index n than those with a narrow gap because of the dependence of n of λ. In the GaAs $-Al_xGa_{1-x}As$ system for instance, n varies as $\Delta n = 0.62\Delta x$ [29], leading to Δn values of the order of a few percent (fig. 2.3(f)). This significant increase in optical confinement over homojunction systems means that losses outside the population inversion region are much reduced, leading to an increase in the confinement factor Γ ($\Gamma = 1 - \exp(-C\Delta nd)$), and hence a decrease in the threshold current. As shown in fig. 2.4, the years following the invention of the double heterostructure laser saw a rapid fall in the room temperature threshold current from $\sim 10^5$ A cm^{-2} for the first DH structures and 500 A cm^{-2} within a few years [30]. In addition, because the high potential barriers are designed to cause carrier confinement, the threshold current is not as temperature sensitive, as shown in fig. 2.5 [31].

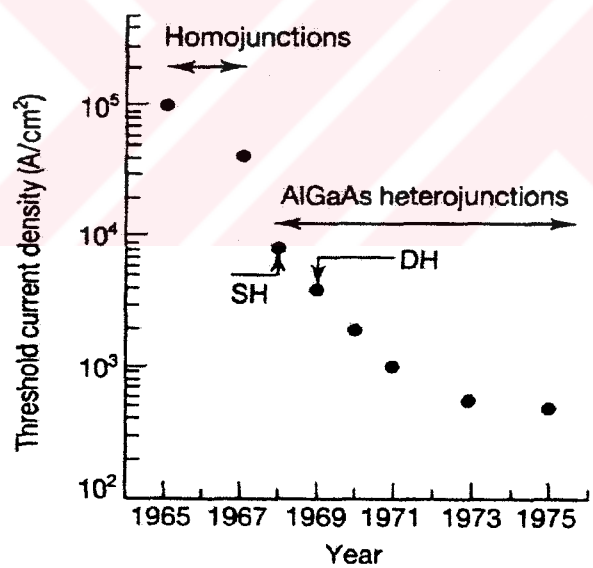

Figure 2.4 Historical trend in threshold current density of early GaAs-based laser diodes [28].

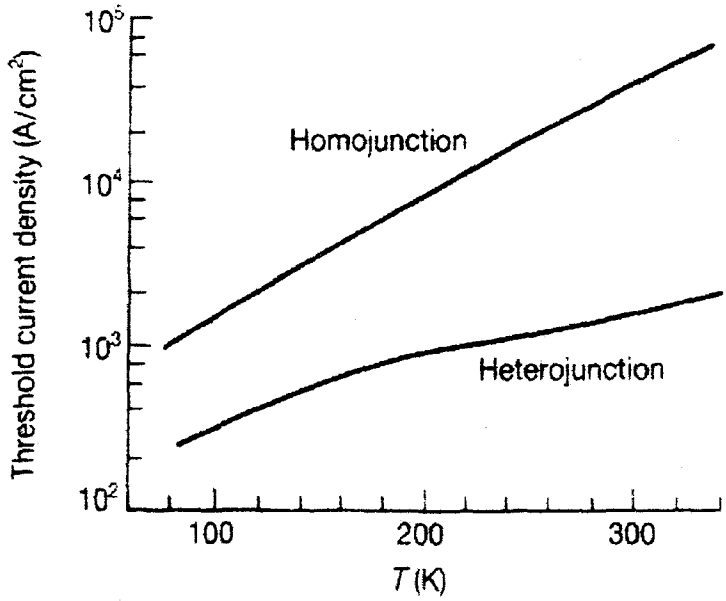

Figure 2.5 A comparison of the threshold current density dependence on temperature for homojunction and heterojunction lasers [28].

2.3 Energy Band Parameters

The discussion so far has centered around a pheneomenological description of band bending with regard to difference in Fermi levels and carrier injection and confinement. One can now readily calculate the differences in E_C and E_V for example using the N-p structure as shown in fig.2.6. Electron affinities χ (the energy required to remove an electron to the vacuum level from the bottom of the conduction band) and work functions φ (similarly defined from the Fermi level) are shown for two separate systems in fig.2.6(a). Note that low band gap materials generally, but not always , have a higher affinity as shown in table 2.1 [32], although it must be said that different sources give variable values for χ, largely due to taking the direct or indirect nature of the band gap without explicitly mentioning it. For instance AlAs is quoted with two band gaps: 2.95 eV gap value. To find the direct gap value, the difference in band gaps is subtracted from this, i.e. direct gap $\chi = (3.5 - (2.95 - 2.16)) = 2.71\,\text{eV}$. From fig.2.6(b), the amount of band bending is given by the difference in the work functions, $\varphi_p - \varphi_N$. Thus the built-in potential of the junction V_{bi} can be given by

$$eV_{bi} = \varphi_p - \varphi_N$$

$$= (E_{gp} + \chi_p - V_p) - (\chi_N + V_N) \qquad (2.3.1)$$

where V_p and V_N are the differences between the Fermi levels and the top of the valence band for the p-material (V_p) or the bottom of the conduction band for the N-material (V_N). Equation (2.3.1) can be reduced to

$$eV_{bi} = E_{gp} + \Delta\chi - (V_p + V_N). \qquad (2.3.2)$$

The conduction band spike ΔE_C has a value given by the electron affinity difference, from fig.2.6(a):

$$\Delta E_c = \chi_N - \chi_p = \Delta\chi. \qquad (2.3.3)$$

Also from fig.2.6(a), the valence band has a discontinuity ΔE_V given by

$$\Delta E_v = (E_{gN} + \chi_N) - (E_{gp} + \chi_p)$$

$$= \Delta E_g - \Delta\chi. \qquad (2.3.4)$$

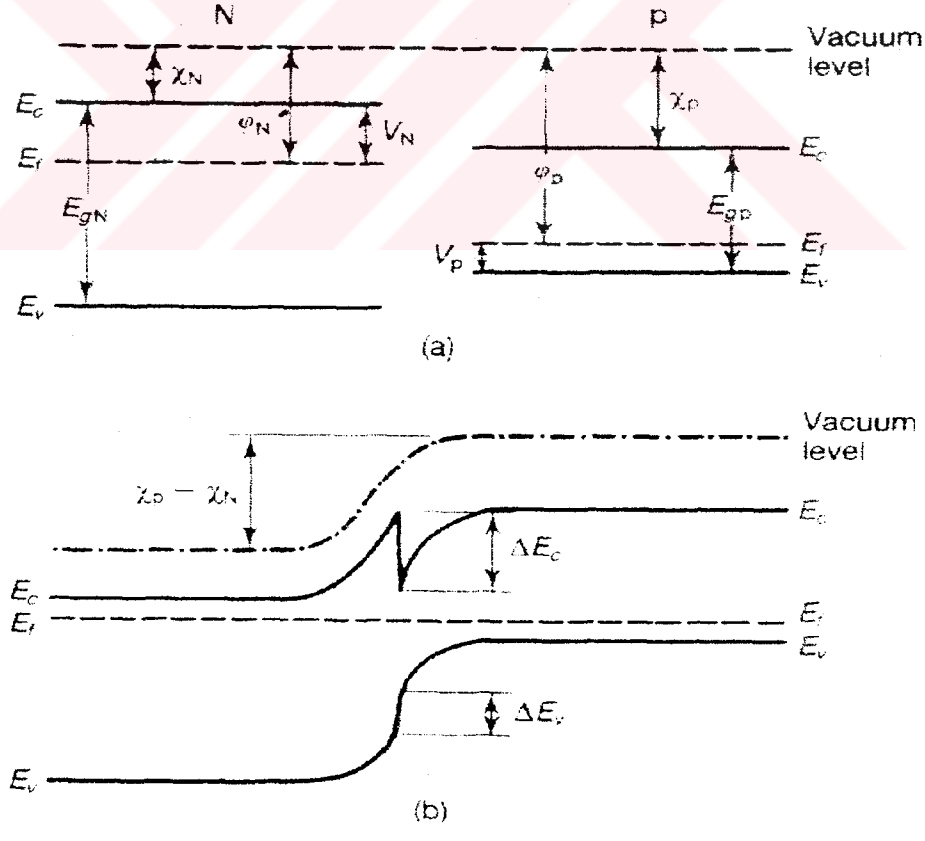

Figure 2.6 Parameters used in the calculation of ΔE_C and ΔE_V in a heterojunction [28].

Combining (2.3.3) and (2.3.4) gives

$$\Delta E_c + \Delta E_v = \Delta E_g \,. \tag{2.3.5}$$

Material	E_g(eV)	χ (eV)
InSb	0.17	4.59
InAs	0.36	4.90
Ge	0.66	4.13
GaSb	0.73	4.06
Si	1.11	4.01
InP	1.35	4.35
GaAs	1.42	4.07
AlSb	1.60	3.65
AlAs	2.16	2.71
GaP	2.25	4.30

Table 2.1 Values of band gap E_g and electron affinity χ for various semiconductors.

2.4 Band Offsets

The band offsets and barrier band gap are important parameters which influence both the quantum well structure and optical confinement factor, and hence the gain. A schematic band energy diagram of a barrier/quantum well structure is shown in fig. 2.7. The energy of the electron potential barrier is determined from the difference ΔE_g between the bulk bandgap energy of the barrier layers and the strained bandgap energy of the active layer multiplied by a dimensioneless conduction band heterostructure discontinuity fraction of $\Delta E_C / \Delta E_g$ as

$$\Delta E_C = \frac{\Delta E_C}{\Delta E_g} \times \Delta E_g \quad \text{or}$$

$$\Delta E_C = Q_C \times \Delta E_g$$

where Q_C is called as conduction band offset ratio. The energy of the hole potential barrier is determined from the same energy difference multiplied by $1 - \Delta E_C / \Delta E_g$.

$$\Delta E_{V} = \left[1 - \frac{\Delta E_C}{\Delta E_g} \right] \times \Delta E_g \quad \text{or}$$

$$\Delta E_{V} = Q_{V} \times \Delta E_g$$

where Q_{V} is called as valence band offset ratio. There is some controversy over what is an appropriate value for the band offset ratios.

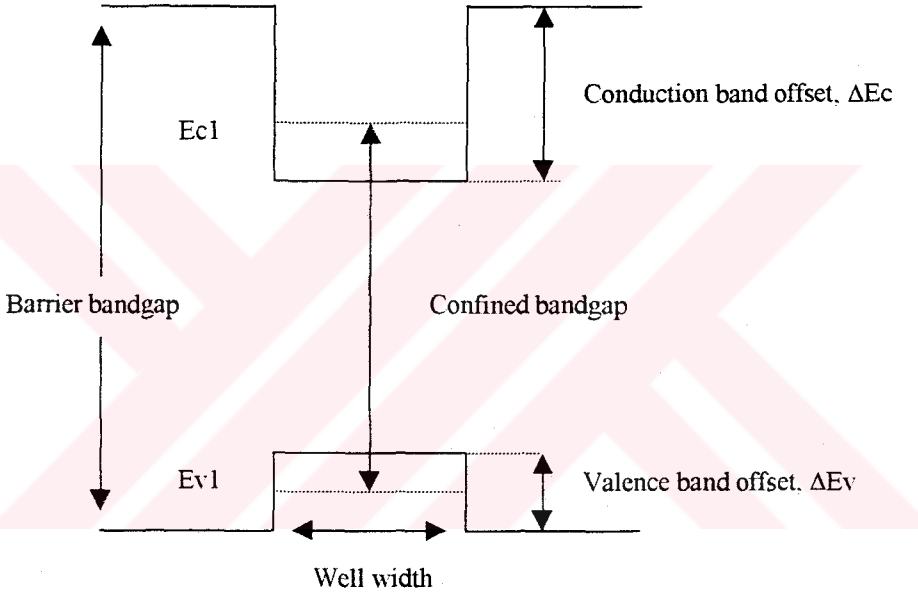

Figure 2.7 Energy band line-up diagram for a quantum well structure. Conduction and valence band offsets are indicated.

The difference between the bandgap of the barriers and the bandgap QW (ΔE_{gap}) is divided between the conduction and valence bands as ΔE_C and ΔE_V, respectively. The ratio $\Delta E_C / \Delta E_V$, termed the band offset ratio, has a characteristic intrinsic value for a particular (QW/barrier) system. For high temperature operation, it is important that $\Delta E_C > \Delta E_V$ because the light effective mass electrons are easily elevated to higher states with increasing temperature. This process both reduce gain and increases the thermal leakage current. In addition, it is important not to have too

large a ΔE_V when a large number of QWs are present in the active region to allow the heavier holes to equally occupy all the QWs [33]. The conventional InGaAsP-InP QW material system has a small ΔE_C / ΔE_V of about 0.67 [34,35], while AlGaInAs-GaAs and InGaasN-GaAs have a ΔE_C / ΔE_V value of around 2.57 and 3.7, respectively [5,34-37], which should result in better electron confinement and equal hole filling in the QWs.

2.5 Band Gap Against Stoichiometry

Various formulae have been put forward to calculate the band gap as a function of *x*. To a first approximation, the variation for a compound $A_{1-x}B_xC$ is linear and is given by

$$E_g(A_{1-x}B_xC) = E_g(AC) + [E_g(BC) - E_g(AC)]x. \qquad (2.5.1)$$

This relationship would be true for any transition, which remained fixed at a given point in *k*-space. However a second-order perturbation of the Schrödinger potential will give a change in E_g proportional to x (1-x). Equation (2.5.1) then becomes

$$E_g(A_{1-x}B_xC) = E_g(AC) + [E_g(BC) - E_g(AC)]x - cx(1-x). \qquad (2.5.2)$$

In its final form

$$E_g(A_{1-x}B_xC) = E_g(AC) + [E_g(BC) - E_g(AC) - c]x + cx^2 \qquad (2.5.3)$$

where c is positive because of the super linear dependence of E_g on x. Equation (2.5.3) was first proposed in [38], where various values of c were calculated-these are reproduced in table 2.2. Note that there will be two versions of (2.5.3) for materials that change from direct to indirect gap: AlGaAs is an example. The values of binary band gaps and c used in calculating the values of the ternary bend gap should always be consistent, i.e. be direct band gap values to calculate Eg for $0<x<0.44$.

Material	c
$Al_xGa_{1-x}As$	0.27
$GaAs_{1-x}P_x$	0.21
$InAs_{1-x}P_x$	0.27
$InAs_xSb_{1-x}$	0.58
$In_{1-x}Ga_xAs$	0.32
$In_{1-x}Ga_xSb$	0.43

Table 2.2 Values of the c parameter for various semiconductors.

2.6 Summary

In this chapter, brief descriptions of single and double heterojunctions, heterojunction lasers and energy bandgap related parameters are presented.

CHAPTER 3

MODEL BAND-OFFSET CALCULATIONS FOR III -V AND NITROGEN CONTAINING III-V SEMICONDUCTOR LASER MATERIAL SYSTEMS

3.1 Introduction

The design and modelling of optoelectronic devices requires a knowledge of various material parameters. What essential is a knowledge of the heterojunction band offset (also known as band discontinuity, band alignment or band line-up), i.e. the relative position of the band edges of the semiconductors constituting the heterojunction. This relative position determines the confinement of the electrons and holes and depends on the composition of the constituents and the amount of strain due to lattice mismatch. Equally important are the band gap energy and the conduction-band and valence-band effective masses. The band gap energy determines the operating wavelength whereas the effective masses determine the electron and hole mobility [1].

The commercially attractive 0.5-4 μm wavelength range may be covered by heterojunction devices which constructed from III-V quaternary alloys. Notably, AlGaInP, AlGaInAs, AlGaAsSb, GaInPAs, GaInAsSb, and InPAsSb. These quaternary alloys include most ternary alloys. A lack of knowledge of the dependence of the various material parameters on alloy composition has hampered a systematic approach to the design of tailor-made optoelectronic devices. The determination band of offsets in particular poses a problem.

Recently it has been recognized that, for the class of III-V semiconductor heterojunctions, the band offset is largely determined by the bulk properties of the semiconductors constituting the heterojunction; band offsets are found to be orientation independent and transitive [2-4]. However, it is in general not possible to measure or calculate bulk band-edge energy levels on an absolute scale. Van de Walle [5] has circumvented this problem by relating the energy levels in bulk semiconductors and he obtained from self-consistent *ab initio* band structure calculations, to a common reference level. This reference level was chosen to be the average electrostatic potential in a semi-infinite 'model-solid'. The model-solid was built up from a superposition of neutral atoms were required to mimic the bulk electron density. This approach also makes it possible to calculate the shift of energy levels due to strain. The model-solid results for the binary constituents and estimates for some of the ternary constituents of the aforementioned quaternary alloys were shown to agree well with the outcome of experiments [2,5].

The aim of this chapter is to review the Model Solid Theory and Harrison's Model which are used to calculate the band offsets of III-V semiconductor laser material systems.

3.2 Calculation of Bulk Band gap with Strain

The average valence-band energy hydrostatic deformation potentials can be obtained for the constituents binary compounds. The bandgap, spin-orbit splitting, and the parameters for calculating the shear deformation potential are obtained from the corresponding experimental data of the binary compounds. Then, an interpolation scheme of expanding the material parameters of ternary and quaternary alloys in fractional constituent ratio x (and/or y) is used to determine the band parameters for lattice matched and strained heterostructures. The interpolation formulas for all physical parameters P used in the calculation of $In_{1-x}Ga_xAs_yP_{1-y}$, $In_{1-x-y}Ga_xAl_yAs$ and $In_{1-x}Ga_xN_yAs_{1-y}$, are given as

$$P(In_{1-x}Ga_xP_{1-y}As_y) = P(GaAs)xy + P(GaP)x(1-y) + P(InAs)(1-x)y - P(InP)(1-x)(1-y) \quad (3.2.1)$$

$$P(In_{1-x-y}Ga_xAl_yAs) = P(InAs)(1-x-y) + P(GaAs)x + P(AlAs)(y) \quad (3.2.2)$$

$$P(In_{1-x}Ga_xN_yAs_{1-y}) = P(GaN)xy + P(GaAs)x(1-y) + P(InN)(1-x)y + P(InAs)(1-x)(1-y) \quad (3.2.3)$$

The material parameters of the binary semiconductors can be found in Table 3.1.The exception to the linear interpolation is the formula for the unstrained bandgap. For $In_{1-x}Ga_xAs_yP_{1-y}$, $In_{1-x-y}Ga_xAl_yAs$ and $In_{1-x}Ga_xN_yAs_{1-y}$ this quantity is given as

$In_{1-x}Ga_xAs_yP_{1-y}$

$$E_g(x,y) = 1.35 + 0.642x - 1.101y + 0.758x^2 + 0.101y^2 - 0.159xy - 0.28x^2y + 0.109xy^2 \text{ (eV)} \quad (3.2.4)$$

$In_{1-x-y}Ga_xAl_yAs$

$$E_g(x,y) = 0.36 + 0.629x + 2.093y + 0.436x^2 + 0.577y^2 + 1.013xy - 2.0xy(1-x-y) \text{ (eV)}. \quad (3.2.5)$$

The bulk band gap energy of $In_{1-x}Ga_xN_yAs_{1-y}$ is calculated by means of band-anti-crossing model which will be presented in section 3.4.

The effects of the strain are calculated in the following way. First, the strain in the plane of the epitaxial growth is

$$\varepsilon = \varepsilon_{xx} = \varepsilon_{yy} = \frac{a_0 - a}{a} \quad (3.2.6)$$

where a is the lattice constant of the quaternary epitaxial layer and a_0 is the lattice constant of the substrate which is assumed to be InP. The strain in the perpendicular direction can be expressed as

$$\varepsilon_{zz} = -2\frac{C_{12}}{C_{11}}\varepsilon \quad (3.2.7)$$

where C_{11} and C_{12} are elastic stiffness constants. The conduction band is shifted by the energy

$$\delta E_c(x,y) = a_c(\varepsilon_{xx} + \varepsilon_{yy} + \varepsilon_{zz}) = 2a_c(1 - \frac{C_{12}}{C_{11}})\varepsilon \tag{3.2.8}$$

and valence bands are shifted by

$$\delta E_{hh}(x,y) = -P_\varepsilon - Q_\varepsilon \tag{3.2.9}$$

$$\delta E_{lh}(x,y) = -P_\varepsilon + Q_\varepsilon \tag{3.2.10}$$

where

$$P_\varepsilon = -a_v(\varepsilon_{xx} + \varepsilon_{yy} + \varepsilon_{zz}) = -2a_v(1 - \frac{C_{12}}{C_{11}})\varepsilon \tag{3.2.11}$$

$$Q_\varepsilon = -\frac{b}{2}(\varepsilon_{xx} + \varepsilon_{yy} - 2\varepsilon_{zz}) = -b(1 + 2\frac{C_{12}}{C_{11}})\varepsilon \tag{3.2.12}$$

where a_c and a_v are the conduction-band and valence-band hydrostatic deformation potentials, and b is the valence-band shear deformation potential.

The strained band gaps can then be expressed as

$$E_{c-hh}(x,y) = E_g(x,y) + \delta E_c(x,y) - \delta E_{hh}(x,y) \tag{3.2.13}$$

$$E_{c-lh}(x,y) = E_g(x,y) + \delta E_c(x,y) - \delta E_{lh}(x,y) \tag{3.2.14}$$

Materials	GaAs	AlAs	InAs	InP	GaP	GaN	InN
Parameters							
a_0 (Å)	5.6533	5.6600	6.0584	5.8688	5.4505	4.503	5.02
E_g (eV)	1.424	3.03	0.354	1.344	2.78	3.40	1.94
deformation potential (eV)							
a_c (eV)	-7.17	-5.64	-5.08	-5.04	-7.14	-2.2	-1.85
a_v (eV)	1.16	2.47	1.00	1.27	1.70	5.2	1.5
b (eV)	-1.7	-1.5	-1.8	-1.7	-1.8	-2.67	-2.67
$C_{11}(10^{11}\text{dyne/cm}^2)$	11.879	12.5	8.329	10.11	14.05	29.6	18.4
$C_{12}(10^{11}\text{dyne/cm}^2)$	5.376	5.34	4.526	5.61	6.203	15.4	11.6
Valence band parameter							
γ_1	6.8	3.45	20.4	4.95	4.05	-	-
γ_2	1.9	0.68	8.3	1.65	0.49	-	-
γ_3	2.73	1.29	9.1	2.35	1.25	-	-
Electron effective mass	0.067	0.15	0.023	0.077	0.25	0. 15	0.14
Heavy-hole effective mass	0.50	0.79	0.40	0.60	0.67	0.855	0.833

Table 3.1 Material parameters for the calculation for InGaAsP, AlGaInAs and GaInNAs material systems.

3.3 Theoretical Models for the Calculation of Band Offsets

The relative alignment of the band edges of the well and barrier material is very important in modelling the band structure. Since experimental measurements for the band offsets in strained QW's remain very difficult, scarce, and uncertain, a theoretical approach must be used to obtain physical reasonable estimations of material parameters for strained QW's. In this section we present two methods of Model Solid Theory and Harrison's Model. With these methods, the band offsets of strained QW's in ternary and quaternary systems are obtainable rather than from

empirical extrapolations of rarely available, scattered and often indirect experimental data for quaternary compounds.

3.3.1 Model Solid Theory

The valence band position of a quaternary is given by [29,30]

$$E_v(x,y) = E_{v,av}(x,y) + \frac{\Delta(x,y)}{3} + \delta E_{hh}(x,y) \quad \text{for hh (compressive strain)} \quad (3.3.1.1)$$

$$E_v(x,y) = E_{v,av}(x,y) + \frac{\Delta(x,y)}{3} + \delta E_{lh}(x,y) \quad \text{for lh (tensile strain)} \quad (3.3.1.2)$$

where $E_{v,av}(x,y)$ is the average valence subband energy and Δ is the spin-orbit split-off band energy. These values are obtained by a linear interpolation of the binary values listed in Table 3.2. The conduction band position may be calculated by simply adding the strained bandgap energy to the valence band position.

$$E_c(x,y) = E_v(x,y) + E_{c-hh}(x,y) \quad \text{for hh (compressive strain)} \quad (3.3.1.3)$$

$$E_c(x,y) = E_v(x,y) + E_{c-lh}(x,y) \quad \text{for lh (tensile strain)} \quad (3.3.1.4)$$

Materials	GaAs	AlAs	InAs	InP	GaP	GaN	InN
Parameters							
Model-solid theory: Average valence-band-edge energy; $E_{v,av}$ (eV)	-6.92	-7.49	-6.67	-7.04	-7.40	-	-
Spin-orbit split-off energy; Δ(eV)	0.34	0.28	0.38	0.11	0.08	0.011	0.006
Harrison's Model: valence-band-edge energy in reference level scale;							
E_{vH} (eV)	0.111	-0.42454	0.441	0.00	-0.388	-	-
E_{cH} (eV)	1.531	2.5255	0.801	1.35	2.352	-	-

Table 3.2 Parameters for the calculation of band alignment of the $In_{1-x}Ga_xAs_yP_{1-y}$, $In_{1-x-y}Ga_xAl_y As$ and $Ga_xIn_{1-x}N_yAs_{1-y}$ material systems.

The conduction band offset is given by

$$\frac{\Delta E_c}{\Delta E_g} = 1 - \frac{E_v^w - E_v^b}{E_g^b - E_g^w} \tag{3.3.1.5}$$

where E_v^w and E_v^b are the valence band positions in the well and barrier materials, respectively, and E_g^w and E_g^b are the strain adjusted band gaps ($E_{c\text{-}hh}$ for compressive strain and $E_{c\text{-}lh}$ for tensile strain) for the well and barrier materials.

3.3.2 Harrison's model

The position of both the conduction and valence bands are determined by [31]

$$E_v(x,y) = E_v^H(x,y) + \delta E_{hh}(x,y) \quad \text{for hh (compressive strain)} \tag{3.3.2.1}$$

$$E_v(x,y) = E_v^H(x,y) + \delta E_{hh}(x,y) \quad \text{for lh (tensile strain)} \tag{3.3.2.2}$$

$$E_c(x,y) = E_c^H + \delta E_c(x,y) \tag{3.3.2.3}$$

where $E_v^H(x,y)$ and $E_c^H(x,y)$ are obtained by a linear interpolation of the binary parameters found in Table 3.2 [19], and $\delta E_{hh}(x,y)$ and $\delta E_{lh}(x,y)$, $\delta E_c(x,y)$ are the strain-induced energy shifts given in (3.2.8-3.2.10). The superscript 'H' refers to Harrison's model. The conduction band-edge discontinuity may then be calculated as

$$\frac{\Delta E_c}{\Delta E_g} = \frac{E_c^{H.b} - E_c^{H.w}}{(E_v^{H.w} - E_v^{H.b}) + (E_c^{H.b} - E_c^{H.w})} \tag{3.3.2.4}$$

where the superscripts w and b indicate the well and barrier materials, respectively.

It should be noted that this method simply is meant to give the parameter $\Delta E_c/\Delta E_g$ which may be used to determine the alignment of the well and barrier materials. The difference between $E_c(x,y)$, $E_v(x,y)$ from equation (3.3.2.1), (3.3.2.2)

and (3.3.2.3) should not be used to calculate the bandgap of the quaternary material. Rather, equation (3.2.4) should be used.

3.4 Band-Anti-Crossing Model

The band-anti-crossing model (BAC) explains the conduction band modification due to the presence of nitrogen in GaInNAs alloys. In this BAC model, an anti-crossing interaction of localized N states with the extended state of GaAs or InGaAs leads to characteristic splitting of the conduction band into two non-parabolic subbands [47]. The downward shift of the lower subband is responsible for the reduction of the fundamental band gap, and optical transitions from the valence band to the upper subband account for the high energy edge. The model has been successfully used to quantitatively describe the dependences of the upper and lower subband energies on N content and on hydrostatic pressure of group III-N-V alloys [48,49-51]. The low energy edges of the subbands are given by the expression

$$E\pm = (E_N + E_M \pm [(E_N - E_M)^2 + 4V_{MN}^2]^{1/2})/2 \qquad (3.4.1)$$

where E_M and E_N are the energies of the extended state and of the N level relative to the top of the valence band , respectively, and V_{MN} (V_{MN} =2.7$\sqrt{y}$ eV, [52] where y is the N composition) is the matrix element of the term describing the interaction between localized N states and the extended states. The predicted splitting of the CB into subbands has been confirmed experimentally [47,53]. The nitrogen level dependences on the nitrogen composition is E_N = 1.52-3.9y [54]. The conduction band energy E_M of the matrix semiconductor is taken to the vary in the presence of nitrogen as $E_M = E_0 - 1.55y$ where E_0 is the energy in the absence of nitrogen [54]. E_- transition shifts towards lower energies with increasing N composition, in contrast, E_+ transition shifts towards higher energies with increasing nitrogen content and its intensity increases relative to the E_- intensity [47,49,53].

As has been stated above, the electron effective mass in III-V-N has been predicted [55,58] to increase with increasing nitrogen composition in the low composition range . This behaviour is rather unusual and is, in fact, opposite to the conventional semiconductors, where the value of the effective mass decreases with

decrease of the band gap energy. Moreover, the CB in the alloys is predicted to be very non-parabolic [57], leading to a strong energy dependence of the effective mass.

3.5 Conclusion

In this chapter we have presented two theoretical models to calculate band lineups for lattice matched and strained-layer interfaces, and tabulated the parameters to calculate the band-offset ratio of the three different semiconductor devices.

CHAPTER 4

THEORETICAL COMPARISONS OF THE BAND-OFFSET RATIOS USING MODEL SOLID THEORY AND HARRISON'S MODEL

4.1 Introduction

This chapter presents the model comparison of the band-offset values for three computing laser structures or InGaAsP, InGaAlAs, and GaInNAs using model solid theory and Harrison's model. We calculate the bulk band gap energy of GaInNAs by means of band-anti-crossing model [59].The element content of each quaternary material are carefully chosen to maximize the conduction band-offset of each material system. Our theoretical study shows that model solid theory can be effectively used to calculate the band offset ratios of the GaInNAs-GaAs for small nitrogen concentration including the effect of strain and modifications in conduction band but neglecting the direct effect of nitrogen.

4.2 Comparison of the Band Models for Phosphide System

A comparison of the model solid theory and Harrison's model for the calculation of the conduction and valence band-offset for InGaAsP-InP structure is shown in fig.4.1. This laser system is uncompensated where compressive strain exists only in active layers. The calculations are obtained both function of the phosphorus concentration and compressive strain in the well, i.e. active layer.

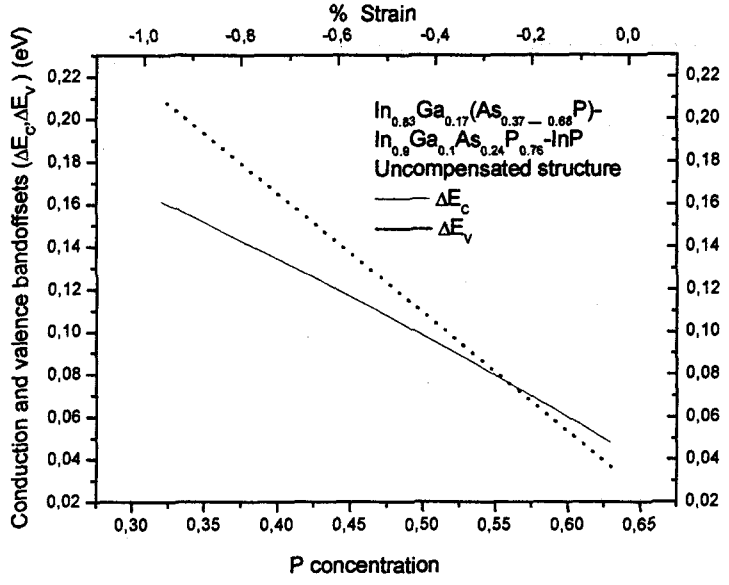

(a)

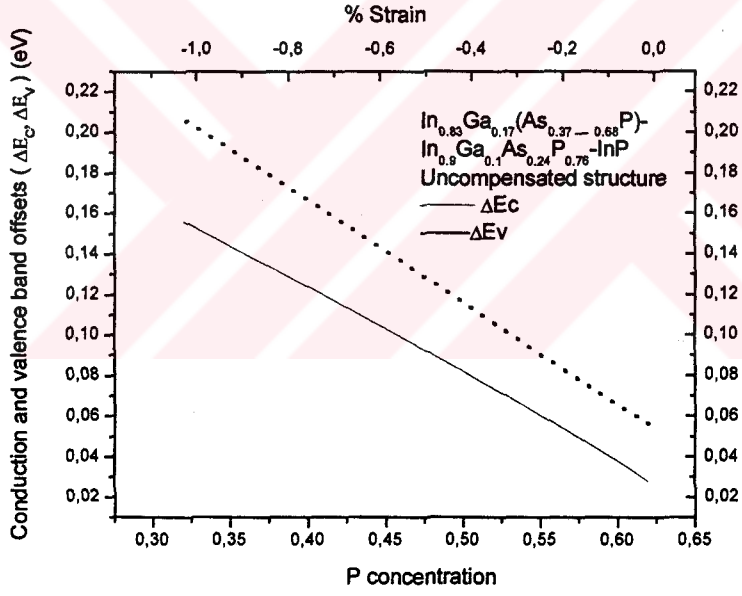

(b)

Figure 4.1 The variation of conduction band-offset ΔE_C and valence band-offset ΔE_V versus P concentration and % strain in well according to (a) Model solid theory and (b) Harrison's model.

The variation of the conduction band-offset ΔE_C and valence band-offset ΔE_V for the InGaAsP-InP uncompensated structure displays similar trend for each model. In both of these figures, conduction and valence band-offsets decrease with

increasing phosphorus P concentration (decreasing compressive strain) and the valence band- offset is deeper than that of the conduction band-offset. This causes low potential barrier height for electrons in the conduction band leading to electron leakage from the quantum well (QW) and reduce the laser performance.

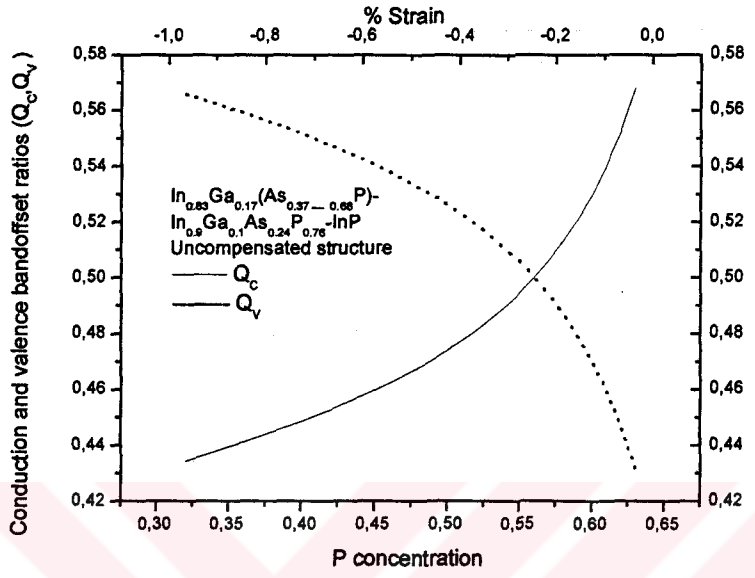

(a)

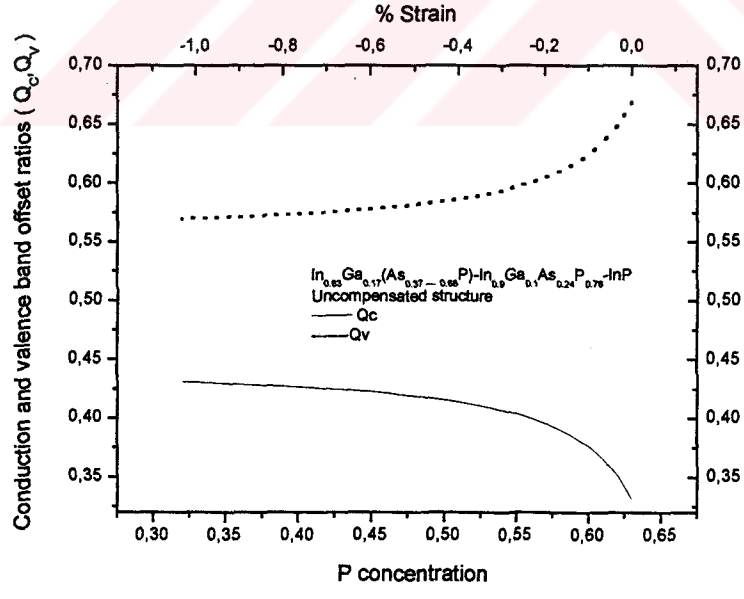

(b)

Figure 4.2 The variation of conduction band-offset ratio Q_C and valence band-offset ratio Q_V versus phosphorus P concentration and % strain in well according to (a) Model solid theory and (b) Harrison's model.

The variation of the conduction band-offset ratio Q_C versus phosphorus P concentration in the well for InGaAsP-InP uncompensated structure displays an opposite trend and it is very dependent on the phosphorus concentration for each model. Conduction band-offset ratio Q_C increases with increasing phosphorus P concentration (decreasing compressive strain in the well) and it is being smaller than that of the valence band-offset ratio for a range of phosphorus concentration of 0.30-0.50 according to model-solid theory however conduction band-offset ratio Q_C decreases with increasing P concentration according to Harrison's model.

The calculated band alignments of InGaAsP-InP by Harrison's model is in good agreement with experimental results [37,45,46,60]. Therefore, to illustrate the effect of the strain-compensation on band offsets we are going to use Harrison's model only. Fig. 4.3 presents the effects of the use of the strain compensated barriers on phosphorus laser structure system. In order to see the influence of strain compensation on band alignments the well compensation is held fixed at $In_{0.83}Ga_{0.17}As_{66}P_{34}$ to allow an emission wavelength of 1.3 μm, on the other hand the arsenide compensation in the barrier is varied. Therefore, the well is compressively strained and the barrier is tensiley strained to compensate the total strain in the laser system. The calculated results of the conduction and valence band offset as a function of both phosphorus concentration and tensile strain in the barrier is shown in fig. 4.3. The investigation of fig. 4.3 shows that the introduction of the compensated barriers brings benefits to this laser structure; (i) both conduction and valence wells get deeper with increasing the tensile strain in the barrier and (ii) valence band offset ratio gets smaller whereas conduction band offset ratio gets bigger with increasing the tensile strain in the barrier. Both of these variations in compensated laser structure improves the band alignment compared to that of the uncompensated laser structure.

The comparison of the figures 4.1 and 4.3 reveals this fact of the introduction of the strain compensated barriers results deeper conduction and valence wells. However, the valence wells are still deeper than that of the conduction bands, which is not advance.

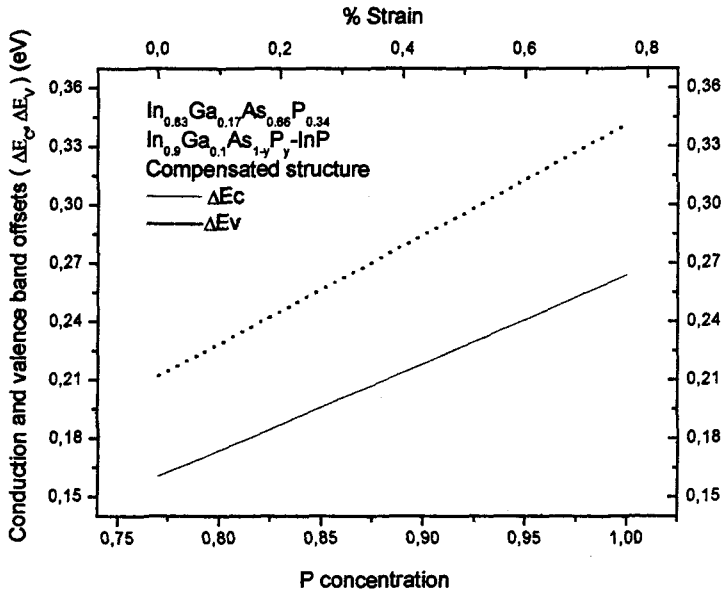

(a)

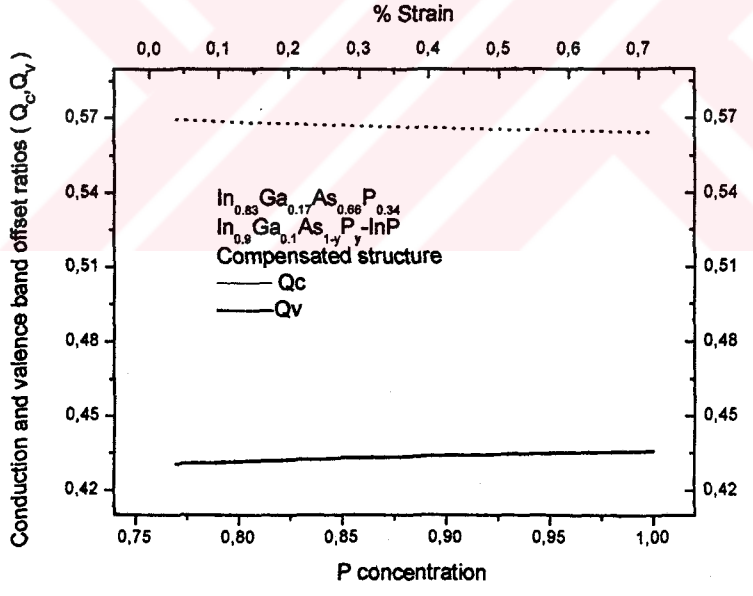

(b)

Figure 4.3 The variation of conduction band offset ΔE_C and valence band offset ΔE_V (a), and the variation of conduction band offset ratio Q_C and valence band offset ratio Q_V (b) versus P concentration and % strain in the barrier according to Harrison's model.

4.3 Comparison of the Band Models for the Aluminium System

A comparison of the model solid theory and Harrison's model for the calculation of the conduction band-offset ΔE_C, and valence band-offset ΔE_V, as a

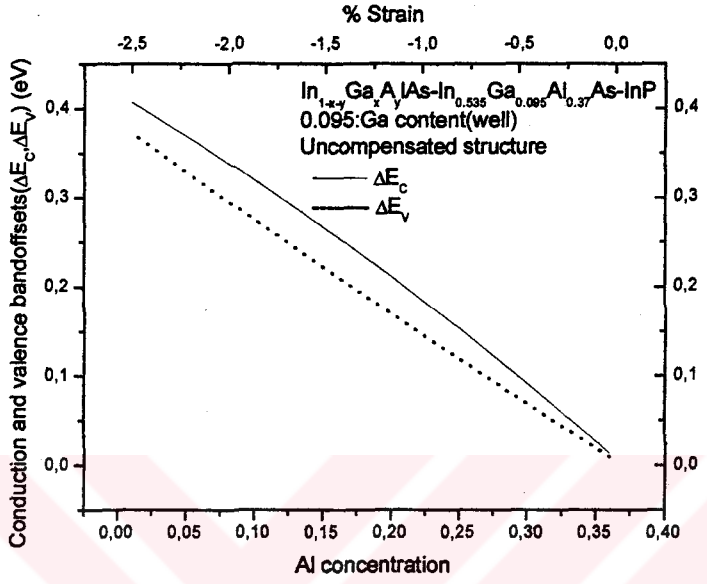

(a)

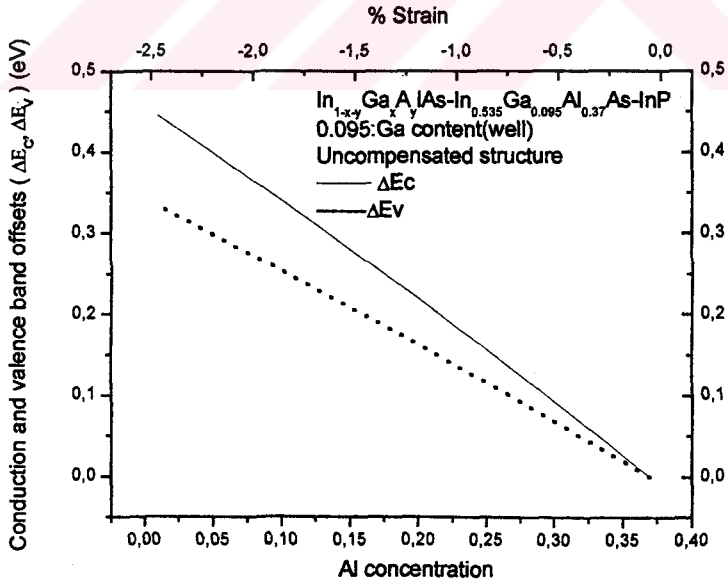

(b)

Figure 4.4 The variation of conduction band-offset ΔE_C and valence band offset ΔE_V versus aluminium Al concentration and % strain in well according to (a) Model solid theory and (b) Harrison's model.

function of both aluminium concentration and compressive strain in the well for function of both aluminium concentration and compressive strain in the well for uncompensated AlGaInAs-InP structure is shown in fig.4.4.

The variation of the conduction band-offset ΔE_C and valence band-offset ΔE_V for the AlGaInAs-InP uncompensated structure displays similar trend for each model as InGaAsP. From these figures, it is clear that AlGaInAs offers a considerably larger conduction band-offset, ΔE_C for lower aluminium concentration (higher compressive strain). Therefore, deeper conduction wells can be achieved by minimizing the aluminium concentration.

Although the variation of the band-offset ratios of Q_C and Q_V versus aluminium Al concentration and compressive strain in the well for AlGaInAs-InP uncompensated structure displays similar trends for each model, the ratios vary quickly with aluminium concentration in model solid theory (see figure 4.5). On the other hand, the rate of the variation of the band offset ratios is very slow in Harrison's model. Valence band-offset ratio is being smaller than that of the conduction band for a range of the aluminium concentration of 0.0 - 0.35 according to two model.

The calculated band alignments of AlGaInAs/GaAs by Harrison's model is in good agreement with experimental results [37,45,46,60,61]. So we will only use the Harrison's model for the rest of the calculations in this laser system. Fig. 4.6 illustrates the use of the strain compensated barriers on conduction and valence band offsets and band offset ratios of the aluminium system. The well composition is held fixed at $Al_{0.175}Ga_{0.095}In_{0.73}As$ and the aluminium concentration and so the tensile strain in the barrier is increased. As can be seen from fig. 4.6 the use of compensated barriers results better band alignment causing deeper conduction and valence wells.

It should be noticed from figures 4.4, 4.5 and 4.6 that the conduction wells are always deeper than the valence wells which is the most significant requirement for high temperature operation.

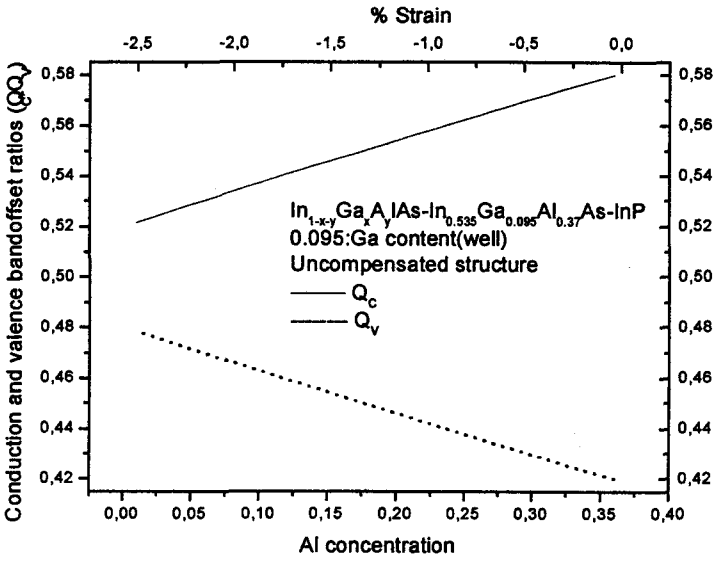

(a)

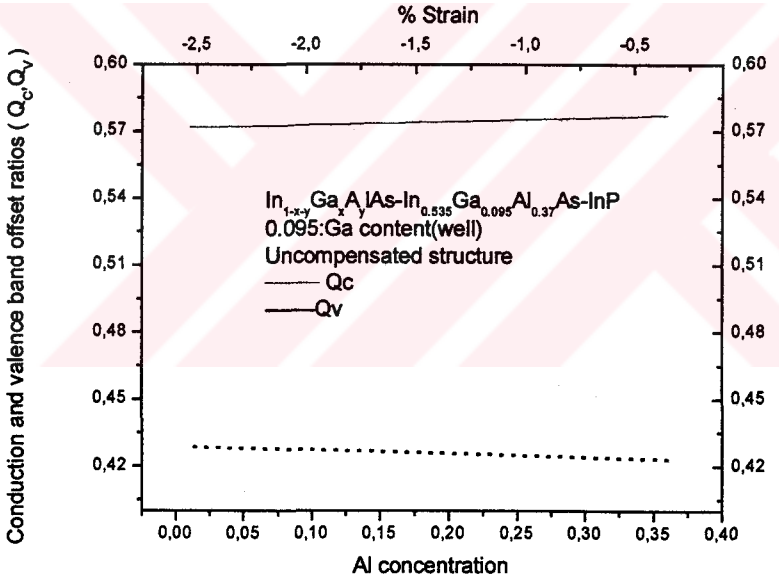

(b)

Figure 4.5 The variation of conduction band-offset ratio Q_C and valence band-offset ratio Q_V versus Al concentration and % strain in well according to (a) Model solid theory and (b) Harrison's model.

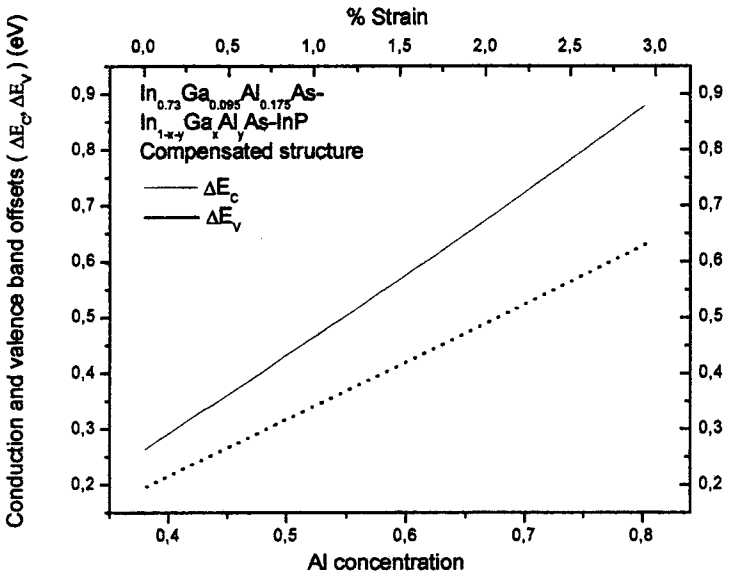

(a)

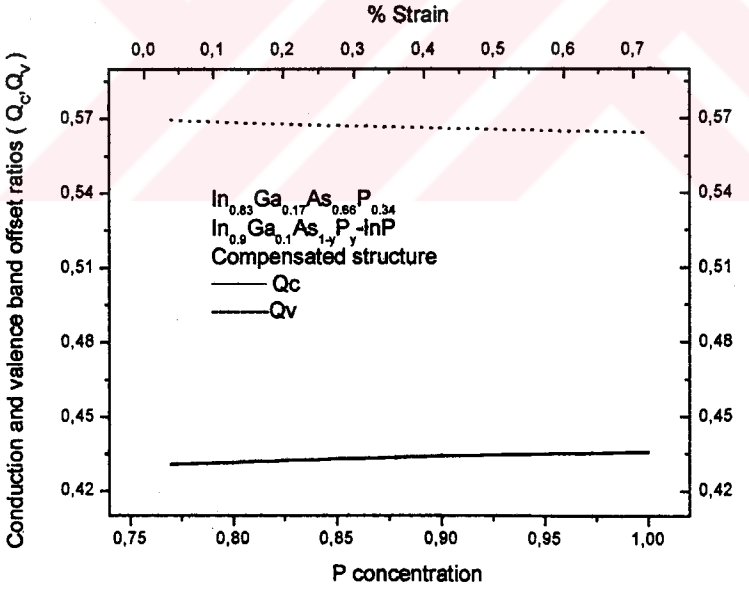

(b)

Figure 4.6 The variation of conduction band offset ΔE_C and valence band offset ΔE_V (a), and the variation of conduction band offset ratio Q_C and valence band offset ratio Q_V (b) versus Al concentration and % strain in the barrier according to Harrison's model.

4.4 Calculation of the Band Alignment of Nitrogen System by Means of Model Solid Theory

Despite strong process in the development of GaInNAs/GaAs devices, detailed spectroscopic studies of the band alignment and electronic states in GaInNAs/GaAs quantum well structures can not be found in the literature to date. There is still exists uncertainty regarding the actual band line up of GaInNAs material systems therefore the experimentally derived data is used for theoretical calculations until now. In this section we showed that the model solid theory can be effectively used to calculate the band alignments of the GaInNAs/GaAs as in the case of strained GaInAs materials. The band alignment between the GaInNAs QW and GaAs cladding is estimated using model solid theory, including the effects of strain but neglecting the direct effect of the nitrogen. We calculate the bulk band bandgap energy of GaInNAs by means of band- anti-crossing model. Fig. 4.7 illustrates the schematic diagram of the bulk bandgap of the GaInNAs alloy system in terms of the band-anti-crossing model. As can be seen from figure 4.7, the bulk bandgap E_+ decreases quickly with increasing nitrogen concentration.

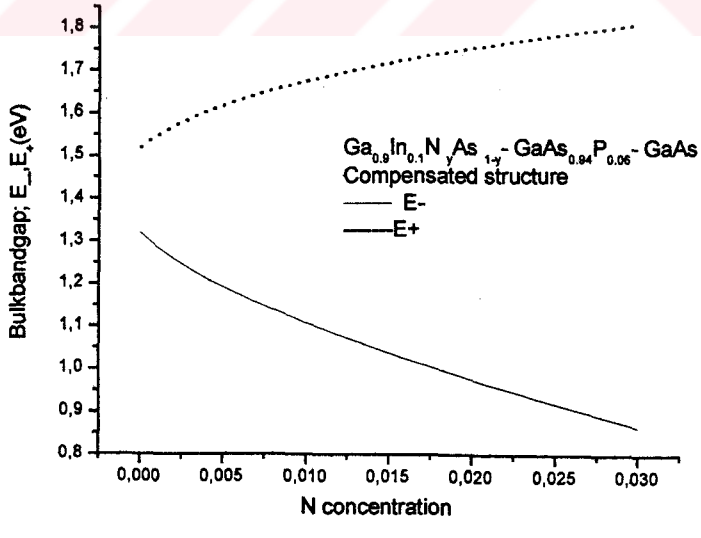

Figure 4.7 Schematic diagram of the bulkbandgap of the GaInNAs alloy, according to the BAC model.

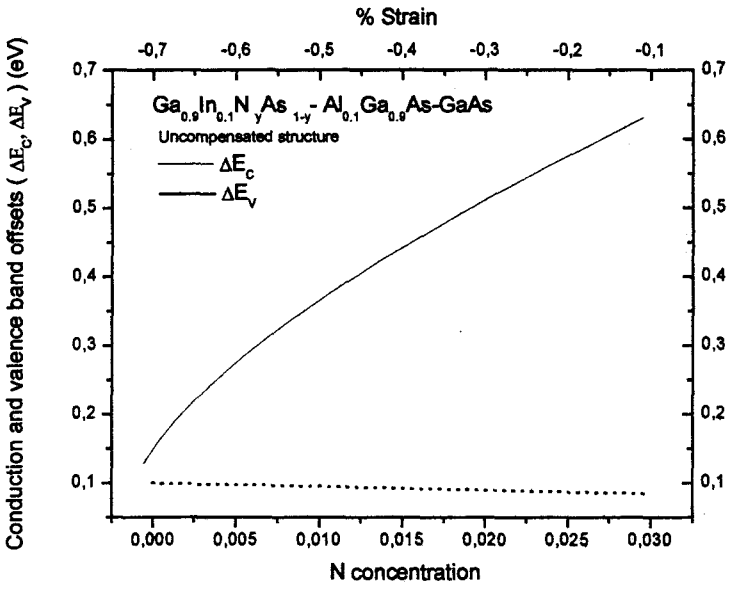

Figure 4.8 The variation of conduction band-offset ΔE_C and valence band-offset ΔE_V versus N concentration and % strain in the well according to Model solid theory.

Figure 4.8 presents the variations of the conduction and valence band offsets with nitrogen concentration (decreasing compressive strain). As it's clear from figure 4.8 that the GaInNAs/GaAs laser system has the favourable band alignment with much deeper conduction wells than that of the valence wells. Fig. 4.9 shows the corresponding band offset ratios for this nitride system. Fig. 4.9 reveals the importance of adding more nitrogen to the system, since Q_V decreases and Q_C increases with increasing nitrogen concentration and such a band alignment improves the temperature dependence of light emitting systems.

It is shown that there is a rapid increase in the conduction band offset when a small fraction of nitrogen is incorporated into InGaAs. This is believed to be caused by interaction of the conduction band with higher-lying N related resonant states[37].

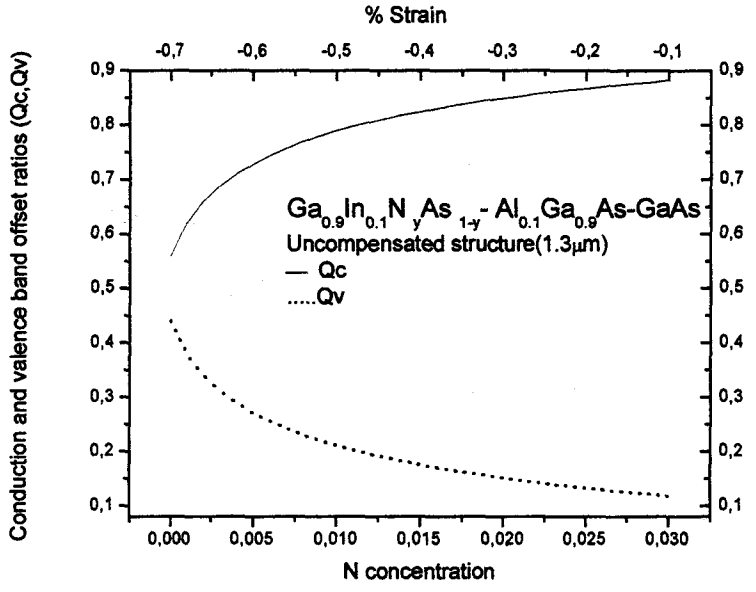

Figure 4.9 The variation of conduction band-offset ratio Q_C and valence band-offset ratio Q_V versus N concentration and % strain in the well according to Model solid theory.

4.5 Conclusions

We have compared the calculated band offset ratios for the three competing laser structure systems of InGaAsP/InP, AlGaInAs/InP and GaInNAs/GaAs. The two theoretical models of 'Harrison's model' and 'Model solid theory' have been used and it is seen that the Harrison's model is in agreement with the experimental results for InGaAsP/InP and AlGaInAs/InP laser systems. We have also shown in this chapter that the band alignment of GaInNAs/GaAs laser structure can be calculated by means of Model solid theory.

It has been shown in all the above three structures that the introduction of the strain compensated barriers improves the band alignment compared to that of the uncompensated system.

CHAPTER 5

A THEORETICAL COMPARISON OF THE BAND-OFFSET RATIOS OF PHOSPHORUS- ALUMINUM- AND NITROGEN-BASED 1.3 μm QW LASERS

InGaAs(P)-InP material system is the most commonly used semiconductor laser system for optical telecommunication applications with emission wavelengths of 1.3 and 1.5 micrometer. However, the practical applications of InGaAs(P)-InP based lasers have been obstructed by its poor characteristics. One of the major problems is the thermal property, which is related to the low potential barrier height in the conduction band [11,12]. For example, the threshold current increases steeply with temperature and the maximum operating temperature becomes limited. This can be explained by the presence of various loss mechanisms of Auger recombination [62], intervalence band absorption [63] and carrier leakage due to the small electron confinement [64]. To overcome these problems alternative improved materials have been sought after. One such material is the AlGaInAs/InP and another strong potential candidate is GaInNAs/GaAs based lasers for future sources in optical communication systems. AlGaInAs/InP strained multiple quantum well (MQW) lasers have been developed to improve temperature dependence in 1.3 μm and 1.5 μm lasers by using wide bandgap barriers for the suppression of the thermal leakage [65,66]. The novel material system, GaInNAs on a GaAs substrate [5,67-69], has several important advantages as compared to the most commonly used InGaAsP/InP systems. First of all, a better high temperature performance of the laser structures is achieved due to a larger conduction band offset and, thus, improved electron confinement and decreased electron spill out at room temperature and above. Secondly, the increase of the electron effective mass with the addition of nitrogen

provides a close match between the effective mass values for electrons and holes, beneficial for laser applications. In addition, GaInNAs gives the flexibility of tailoring the bandgap and an increase in the lattice parameter. Hence GaInNAs gives the potential to produce material lattice matched or mismatched to GaAs with a wide range of bandgap energies (from ≈ 1.5 eV to less than 0.8 eV) [70]. This provides a possibility of using low cost GaAs substrate as a viable alternative to the dominating InP based heterostructure lasers. Reduced Auger recombination may also occur as a result of the larger electron effective mass and the strong non-parabolicity of the conduction band. In these alternative systems of AlGaInAs/InP and GaInNAs/GaAs, the conduction band offset ratio is greater than 0.5, which is expected to lead to a stronger electron confinement. Therefore, these results in the laser properties of these new materials becoming less temperature dependent than that of the InGaAsP/InP based lasers.

In order to maintain high material gain from a QW, a number of factors have to be taken into consideration [71]. It has been demonstrated that to obtain low transparency carrier density (for low lasing threshold) and high differential gain (for high speed modulation), the QW has to be designed in such a way that there exists a density of states that is as low as possible and a closely matched density of states in the valence and conduction bands. This is very dependent on band offsets. The penalty for a low density of states is that the Fermi level rises rapidly with temperature; hence high QW barriers are required. The amount of strain in the QW influences the material gain as well. The band offsets also play a role in reducing thermal escape of carriers. A large value of ΔE_c will improve the electron confinement, especially at high temperature and this will lead to improved gain due to the light electron masses. In addition, it is important not to have too large a ΔE_v when a large number of QWs are present in the active region to allow the heavier holes to equally occupy all the quantum wells. Therefore, there needs to be a balance between all these criteria for good gain. Increasing the band offsets lead to improved gain, but a balance between the density of states that exists in the QW (both electron and hole states) is still required [71].

For modelling semiconductor quantum well structures, the relative band alignment of the band edges between the quantum well and the barrier is very important. This is rather complicated for the strained case. The calculated band

alignments of InGaAsP/InP and AlGaInAs/GaAs by Harrison's model [45,46,60] are in good agreement with experimental results [37]. However, despite strong progress in the development of GaInNAs/GaAs devices, hardly and detailed spectroscopic studies of the band alignment of GaInNAs/GaAs quantum well structures can be found in the literature to date. Therefore the experimentally derived data [37] is used in literature for gain calculations. Recently, Lin et al. [72] used the model solid theory for GaInNAs/GaAs as in the case of strained GaInAs materials. In this paper, we present calculations which show that the model solid theory can be effectively used to calculate the band alignments of GaInNAs/GaAs ignoring the presence of nitrogen in the average valence band edge energy values and taking into account the presence of nitrogen for the other all laser parameters. We calculate the bulk band gap energy of GaInNAs by means of band-anti-crossing model [59].

To date, GaInNAs semiconductor alloy is being intensively studied for both its fundamental properties [47,73] and its potential applications for 1.3 μm laser applications [74,75]. It has been reported that the incorporation of nitrogen in GaInNAs can reduce the bandgap energy and allows emission wavelengths as long as 1.3 μm to be reached [75]. However, the optical material quality deteriorates significantly with increasing N mole fractions [76], resulting in a much higher threshold current density of GaInNAs/GaAs lasers compared with that of GaInAs/GaAs lasers. In order to improve the performance of 1.3 μm GaInNAs/GaAs quantum well lasers, the nitrogen composition of GaInNAs well should be reduced, although, this leads to an increased strain in the quantum wells. By introducing a strain compensated barrier to this system it is possible to grow highly strained GaInNAs wells free of misfit dislocations. In strain-compensated QWs opposite strains are introduced in the well and barrier regions. These opposite strains balance each other and the average strain in the structure is reduced. In addition, for some laser configurations, such as short cavity lasers or distributed Bragg reflector lasers, a large number of QWs may be required for optimal performance [77]. As the number of strained QWs is increased, the total strain in the structure accumulates and the total strained layer thickness approaches a critical thickness at which lattice misfit dislocations start to form [78]. In strain compensated QWs, the well width and the total number of wells can thus be increased, leading to an enhanced optical confinement. By means of introducing strains of opposite signs in the well and

barrier layers to simultaneously vary the offsets of the heavy- and light-hole states, it is also possible to reduce the mixing between heavy- and light-hole states by means of spatially separating them to different layers [79]. Therefore, there has been an interest in strain compensated quantum well structures. Experimental results [26,80] showed that the strain compensated QW lasers are desirable for optical applications with low threshold current and high efficiency. Therefore, this work investigates how the unique features of GaInNAs/GaAs quantum wells offer the best band alignment compared to conventional InGaAsP/InP and AlGaInAs/InP QW lasers. We use Harrison's model to determine the band-alignment of InGaAsP/InP and AlGaInAs/InP and model solid theory to determine the band-alignment of GaInNAs/GaAs laser systems. By means of these two models we also investigate the effect of the strain compensation on band-alignments for the three competing laser systems. These calculations provide the first clear comparison of the band-alignment of three competing 1.3 μm laser systems and will enable us to predict the effect of the strain-compensation on band-offset energies for quantum well laser structures. For the band structures of laser systems, the material parameters except for the electron effective mass and band gap energies are linearly interpolated from those of binary materials [46,81].

We consider three different laser structures operating around 1.3 μm wavelengths for comparison. The first type of device studied is P-based lasers which consists of $In0.83Ga0.17As1_{-y}P_y$ / $In_{0.9}Ga_{0.1}As_{0.24}P_{0.76}$ / InP with unstrained barriers. We vary the y concentration between 0.32 and 0.63 to get an emission wavelength range of about 1.3-1.0 μm. Figure 5.1 presents the band offset ratios for P-based uncompensated system according to Harrison's model. As can be seen from these variations that the valence band VB offset ratio is greater than that of the conduction band CB with an increase in phosphorus P concentration that results compressive strain. The conduction and valence band offsets as a function of phosphorus concentration and compressive strain in the well is shown in fig. 5.2.

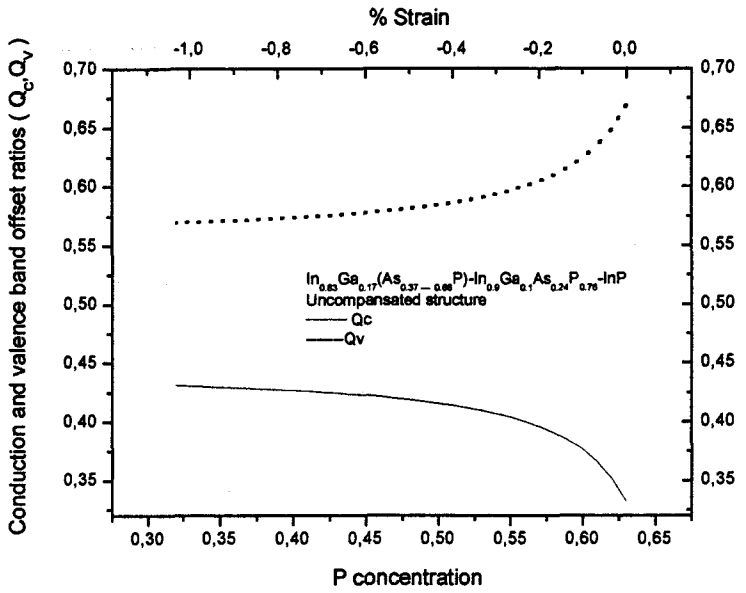

Figure 5.1 The phosphorus concentration (in well) dependence of the conduction and valence band offset ratios of the uncompensated $In_{0.83}Ga_{0.17}As_{1-y}P_y/In_{0.9}Ga_{0.1}As_{0.24}P_{0.76}$/InP laser system according to Harrison's model.

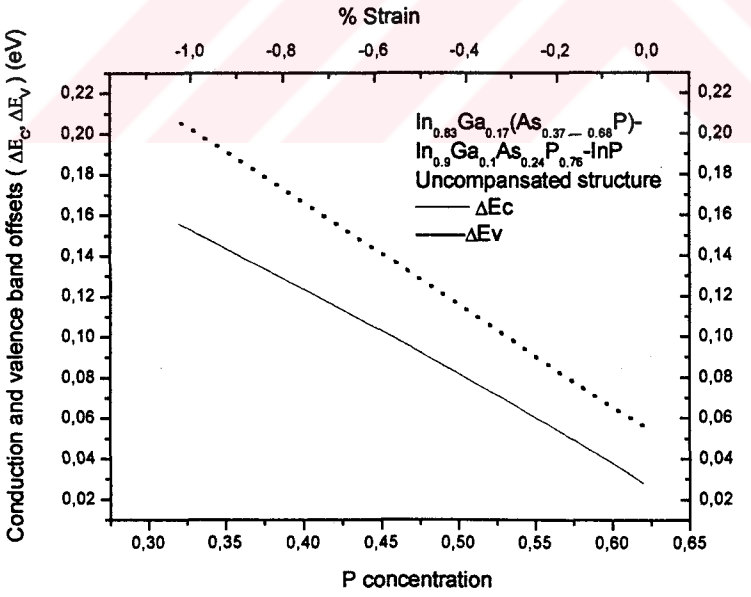

Figure 5.2 The variation of the conduction and valence band offsets with phosphorus concentration and compressive strain (in well) for uncompensated $In_{0.83}Ga_{0.17}As_{1-y}P_y/In_{0.9}Ga_{0.1}As_{0.24}P_{0.76}$/InP laser system according to Harrison's model.

The amount of the compressive strain in the well decreases with increasing P concentration. Therefore, increasing the strain in the well increases the band offsets. However, the VB is deeper than that of the CB leading to poor characteristics. Strain compensation gives access to a wider range of material composition, and thus improved possibilities to select band-edge offsets tailored to specific device needs [82].

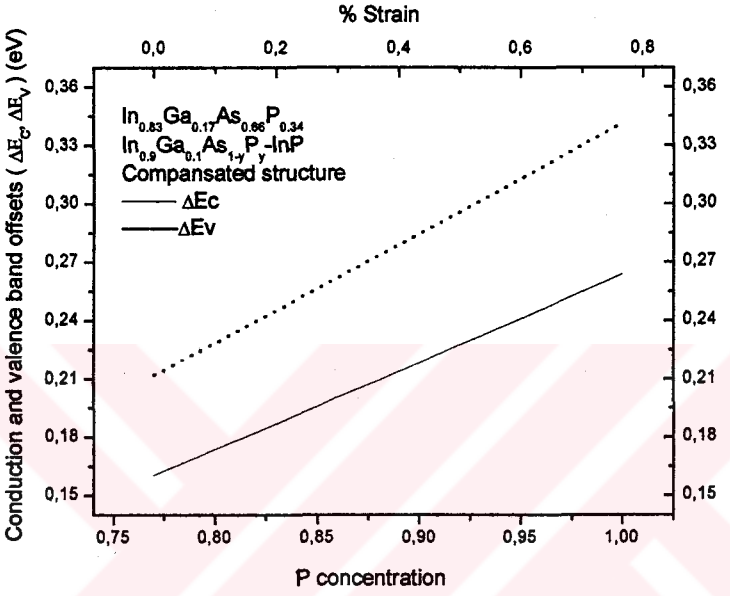

Figure 5.3 The calculated variation of the conduction and valence band offsets with phosphorus concentration and tensile strain (in barrier) for compensated $In_{0.83}Ga_{0.17}As_{0.66}P_{0.34}$ / $In_{0.9}\ Ga_{0.1}\ As_{1-y}\ P_y$ / InP laser system according to Harrison's model.

Fig. 5.3 illustrates the effect of the strain-compensation on band-offsets for P-based system. The well composition is kept as $In_{0.83}Ga_{0.17}As_{0.66}P_{0.34}$ to allow an emission wavelength of 1.3 μm. The phosphorus y concentration of the barrier of $In_{0.9}\ Ga_{0.1}\ As_{1-y}\ P_y$ is varied to compensate the compressive strain in the well. As can be seen from fig. 5.3 by strain compensating with opposite strain in the barrier, it is possible to get deeper wells leading to much better confinement both in CB and VB. Therefore, strain-compensation has significant effect on the band offsets although the VB energies are still greater than that of the CB.

The second type of device is Al-based lasers with $Al_yGa_xIn_{1-x-y}As$ / $Al_{0.37}Ga_{0.095}In_{0.535}As$ / InP structure parameters; gallium content in the well is kept at

0.095 and aluminium concentration is varied between 0.01-0.37 which leads compressive strain.

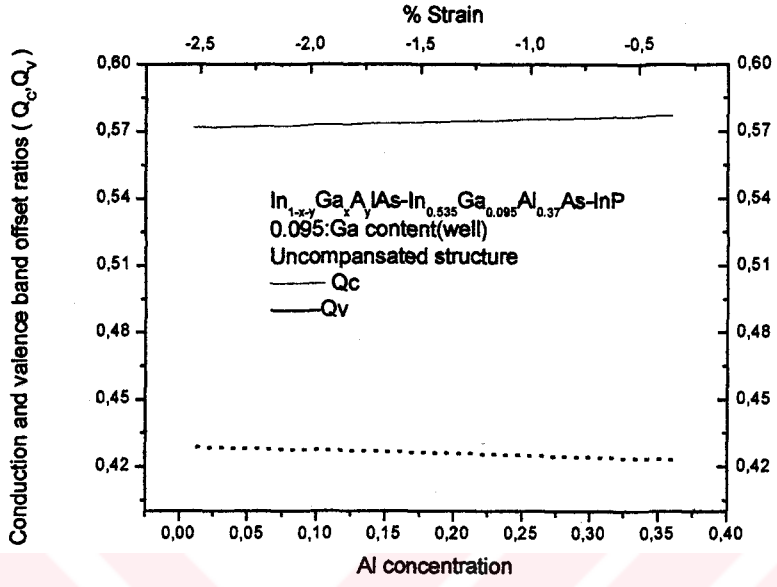

Figure 5.4 The aluminium concentration (in well) dependence of the conduction and valence band offset ratios of the uncompensated $Al_yGa_xIn_{1-x-y}As/Al_{0.37}Ga_{0.095}In_{0.535}As/InP$ laser system according to Harrison's model; gallium content in the well is kept at 0.095.

Fig. 5.4 illustrates the band offset ratios for Al-based laser system using again Harrison's model. Adding aluminium to InGaAs decreases the compressive strain in the well. The emission wavelength of 1.3 μm corresponds to Al concentration of $\approx$17.5% (1.3% compression). A comparison of Al-system with that of the P-system emitting at 1.3 μm shows that their band-offset ratios are similar. On the other hand, the calculated band offsets for Al-system, as shown in fig. 5.5, has improved compared to that of the P-system of fig. 5.2. First, CB offset in Al-system is higher than that of the VB offset as opposed to P-system. Second, both the CB and VB wells are deeper in Al-system. So this variation proves clearly that the Al-system has favourable band offset and it can preferred due to this property compared to P-system.

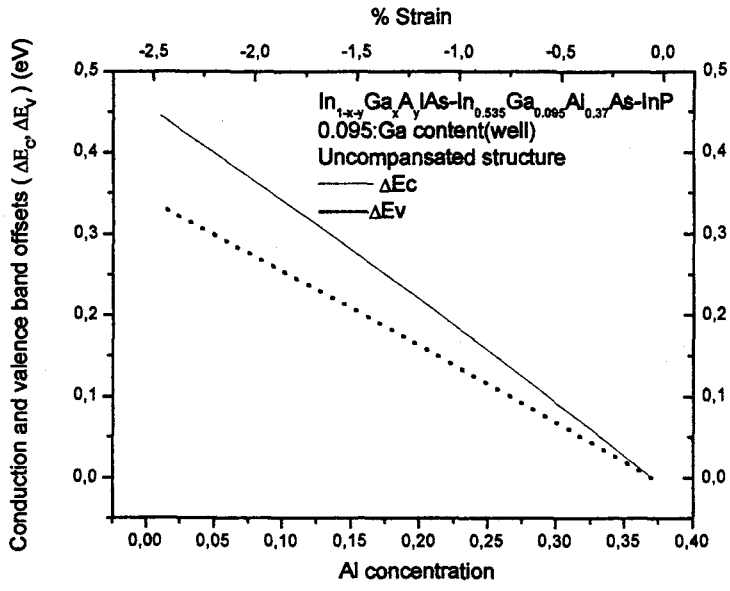

Figure 5.5 The variation of the conduction and valence band offsets with aluminium concentration and compressive strain (in well) for uncompensated $Al_yGa_xIn_{1-x-y}As/Al_{0.37}Ga_{0.095}In_{0.535}As/InP$ lasers system according to Harrison's model; gallium content in the well is kept at 0.095.

However, it should be noticed that adding Al to InGaAs decreases band offset energies at the expense of reducing strain and the difference in band offset gets smaller with decreasing strain. Therefore, in order to have much deeper CB's than that of the VB one should keep the Al concentration as low as possible and this leads to the problem of the critical thickness. At this point, strain-compensation can be offered as a solution to this system. To see the effect of the strain compensation on the band alignments of Al-based lasers, we keep the well composition fixed at $Al_{0.175}Ga_{0.095}In_{0.73}As$ to allow an emission wavelength of 1.3 μm and vary the Al concentration in the barrier as shown in fig. 5.6. Strain-compensation brings further improvements to this favourable laser system as shown in fig. 5.6.

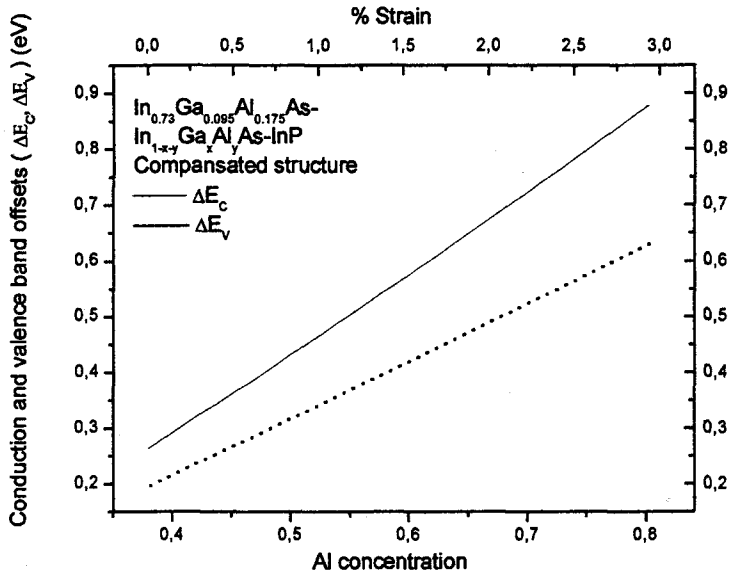

Figure 5.6 The calculated variation of the conduction and valence band offsets with aluminium concentration and tensile strain (in barrier) for compensated $Al_{0.175}Ga_{0.095}In_{0.73}As$/ $Al_yGa_xIn_{1-x-y}As$ / InP laser system according to Harrison's model; x=0.095.

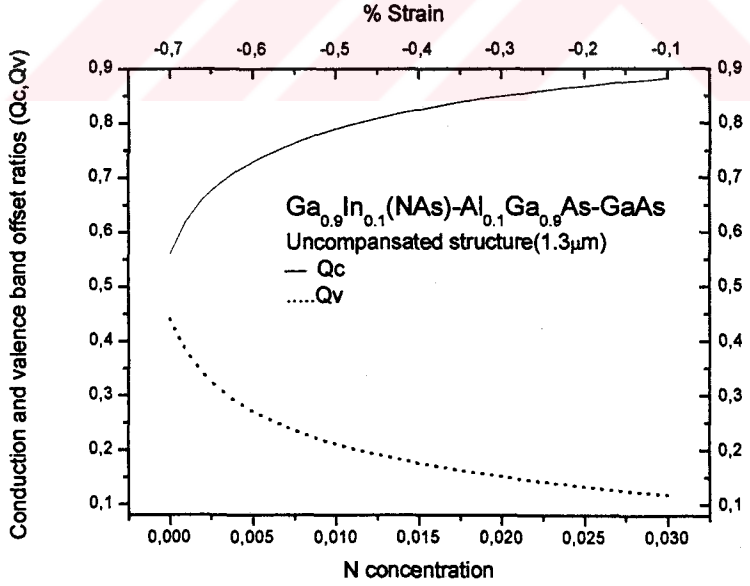

Figure 5.7 The nitrogen concentration (in well) dependence of the conduction and valence band offset ratios of the uncompensated $Ga_{0.9}In_{0.1}N_yAs_{1-y}$ /$Al_{0.1}Ga_{0.9}As$/GaAs laser system according to model solid theory.

The third type of device is an N-based laser with compressively strained $Ga_{0.9}In_{0.1}N_yAs_{1-y}$ quantum wells between $Al_{0.1}Ga_{0.9}As$ barriers and GaAs cladding layers.

Fig. 5.7 presents the band offset ratios for uncompensated N system with AlGaAs barriers by means of model solid theory. The addition of N to InGaAs causes substantial changes in the band alignments; adding N to InGaAs increases the CB offset and decreases the VB offset. The usual $\Delta E_c / \Delta E_v$ ratio changes from 1.2 to around 7 with an addition of 3% nitrogen. At first a rapid and then a gradual change in band offsets have been calculated. The corresponding band offsets are

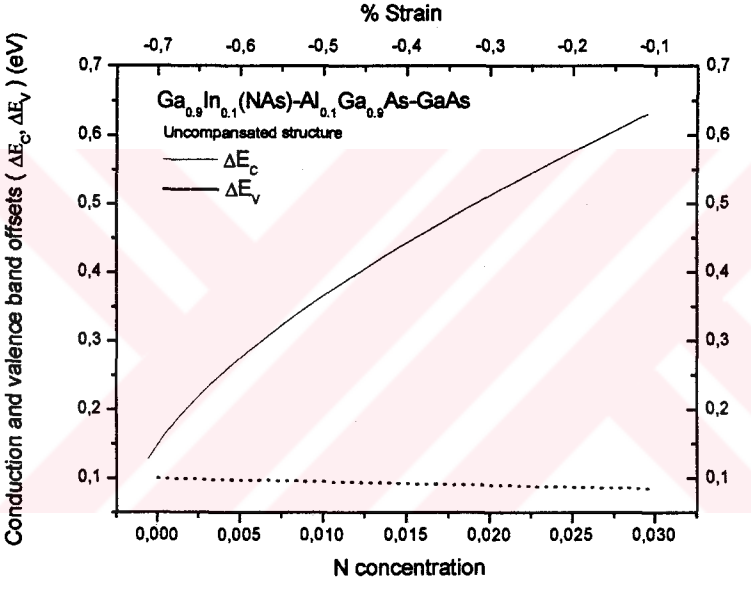

Figure 5.8 The variation of the conduction and valence band offsets with nitrogen concentration and compressive strain (in well) for uncompensated $Ga_{0.9}In_{0.1}N_yAs_{1-y}$ / $Al_{0.1}Ga_{0.9}As$ / GaAs laser system according to model solid theory.

shown in fig. 5.8 which illustrates the fact that the addition of nitrogen into InGaAs leads the N-system having a band alignment of that of the ideal case (deep C wells and shallow V wells) certainly. In addition, these calculations indicate that the band alignment of the N system can be calculated effectively by means of model solid theory since the calculated results are in agreement with that of the experimental results.

On the other hand, the addition of nitrogen deteriorates laser parameters, so one should keep the N composition as low and low N leads high strains. So strain

compensation again can be offered as a solution in this novel material system as well and this can be achieved by means of using GaAsP barriers instead of AlGaAs barriers. The well composition is held fixed as $Ga_{0.9}In_{0.1}N_{0.025}As_{0.975}$ and the tensile strain in the barrier is varied from 0 to 0.7 %, see fig. 5.9.

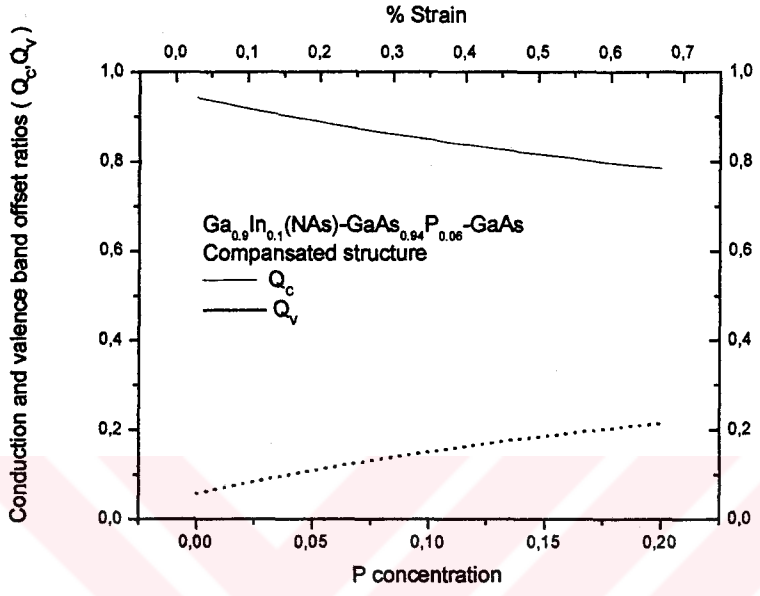

Figure 5.9 The variation of the conduction and valence band offset ratios with phosphorus concentration and tensile strain (in barrier) for compensated $Ga_{0.9}In_{0.1}N_{0.025}As_{0.975}$ /$GaAs_{1-y}P_y$ /GaAs laser system according to model solid theory.

The uncompensated system corresponds to zero strain in the barrier. First, it should be noticed from the variations of fig. 5.9 that using GaAsP barriers instead of AlGaAs barriers improves the band alignment even in the uncompensated value. Second, Q_C value is much higher than the Q_V for uncompensated value and the compensation decreases the Q_C and increases the Q_V value. Therefore the compensation can be thought as to bring disadvantageous to the system. Fortunately, this is not the case. Although Q_C and Q_V show opposite trend with compensation, both conduction- and valence-band offsets increases with compensation, see fig. 5.10.

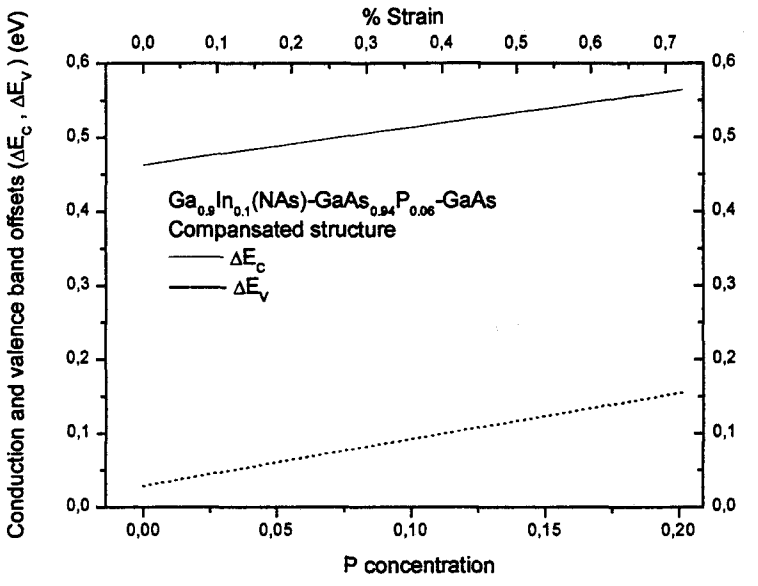

Figure 5.10 The calculated variation of the conduction and valence band offsets with phosphorus concentration and tensile strain (in barrier) for compensated $Ga_{0.9}In_{0.1}N_{0.025}As_{0.975}/GaAs_{1-y}P_y$ /GaAs laser system according to model solid theory.

This strange behaviour of the increase of ΔE_c with decreasing Q_C can be explained as follows; the variation of the conduction band offset is a result of the combined effect of the variation of Q_C and ΔE_g since $\Delta E_c = Q_c \Delta E_g$ and ΔE_g is the difference of the strained bandgap of the barrier and well. The rapid increase in $\Delta E_g (= E_{g_{barrier}} - E_{g_{well}})$ with P concentration eliminates the effect of the decrease in Q_C with increasing P concentration and as overall results an increase in ΔE_c with increasing P concentration. So compensation brings further improvements to the N system. This can be considered as another intrinsic superior property of the N system.

In conclusion, theoretical calculations have been presented to compare the band alignments of typical three competing laser devices emitting in the neighbourhood of 1.3 μm. We have shown that model solid theory can be used effectively to calculate the band alignments of N-based lasers where only experimental data available to date. The investigation of the band alignments of the three competing laser devices indicates that Al- and N-based laser systems are

superior to that of the P-based laser system and offers N-based laser system as an ideal candidate for high temperature operation.

CHAPTER 6

CONCLUSIONS

The work carried out in thesis considered the effects of strain (i) only in the well and (ii) both in the well and barrier on the band alignment of the three competing laser devices of InGaAsP/InP, AlGaInAs/InP, and GaInNAs/GaAs. Our theoretical calculations show how the required band alignment can be obtained by means of changing the well composition in each system.

We have shown that model solid theory can be used to calculate the band alignment of the GaInNAs/GaAs laser structure system where only experimentally derived data is available until now. The band alignment between GaInNAs well and GaAs cladding layer can be estimated including the effects of strain and modifications in conduction band due to the nitrogen but neglecting the direct effect of nitrogen in the average valence band energy values.

The comparative study of the three competing laser devices reveals the fact that AlGaInAs and GaInNAs laser systems have substantially better band alignment than that of commonly used InGaAsP laser system. The calculations show that AlGaInAs proves to be preferred with its favourable band offset compared to InGaAsP. In addition, GaInNAs has the best band alignment due to its larger conduction band offset and reasonable valence band offset.

The theoretical calculations also reveals the fact that the use of strain compensated barriers in all of the three competing laser structure bring further improvements in the band alignment of each laser system.

REFERENCES

[1] E. P. O'Reilly and M. Silver, *Appl. Phys. Lett.* **63** (1993) 3318.

[2] J. O'Gorman, A. F. J. Levi, T. Tanbun-Ek, D. L. Coblentz, and R. A. Logan, *Appl. Phys. Lett.* **60** (1992) 1058.

[3] C. Silfvenius, G. Landgren, and S. Marcinkevicius, *IEEE J. Quantum Electron.* **35** (1999) 603.

[4] B. Chen, W. Wanf, X. J. Wang, J. Y. Zhang, and Z. Fan, *Jpn. J. Appl. Phys.* **38** (1999) 5096.

[5] M. Kondow et all. , *Jpn. J. Appl. Phys.* **35** (1996) 1273.

[6] B. Zhao, T. R. Chen, A. Shakouri, and A. Yariv, *Appl. Phys. Lett.* **63** (1993) 432.

[7] R. Dingle and C. H. Henry, '*Quantum effects in heterostructure lasers*', U. S. Patent 3 982 207, 1976

[8] W. T. Tsang, C. Weisbuch, R. C. Miller, and R. Dingle, *Appl. Phys. Lett.* **35** (1979) 673.

[9] W. T. Tsang, *Appl. Phys. Lett.* **39** (1981) 786.

[10] P. S. Zory, Jr. (Ed.), *Quantum Well Lasers*. Orlando, FL:Academic, 1993.

[11] M. S. Hybertsen, *Appl. Phys. Lett.* **58** (1991) 1759.

[12] R. F. Kazarinov and H. R. Pinto, *IEEE J. Quantum Electron.* **30** (1994) 49.

[13] G. L. Belenky et al., *IEEE Trans. Electron Device*, to be published.

[14] P. J. A. Thijs et al., *in Proc. 17th European Conf. Opt. Commun.*, Paris, Sept. 9-12 (1991) 48.

[15] C. E. Zah et al., in OFC 94 Tech. Dig., **4** (1994) 204.

[16] W. Li, T. Jouhti et al., *Appl. Phys.. Lett.* **79** (21) (2001) 3386.

[17] W. Shan, W. Waluekiewicz et al., *Phys. Rev. Lett.* **82** (1992) 1221.

[18] B. Borchert, A. Y. Egorov, S. Illek, H. Riechert, *IEEE Photon Technol Lett.* **12** (2000) 597.

[19] C. S. Peng, T. Jouhti et al., *IEEE Photon Technol Lett.* **14** (2002) 275.

[20] M. Bissiri, V. Gaspari et al., *Appl. Phys. Lett.* **79** (2001) 2585.

[21] C. Skierbiszewski, P. Perlin et al., *Appl. Phys. Lett.* **76** (2000) 2409.

[22] S. D. Offsey, W. J. schaff, L. F. Lester, L. F. Eastman, and S. K. Mckernan, *IEEE J. Quantum Electron.* **QE-27** (1991) 1455.

[23] P. J. Thijs, L. F. Tiemeijer, P. I. Kuindersman, J.J. Binsma, and T.V. Dongen, *IEEE J. Quantum Electron.* **QE-27** (1991) 1426.

[24] H. Asonen, A. Ovtchinnikov, et al., *IEEE J. Quantum Electron*, **30** (1994) 415.

[25] J. J. Coleman, K. H. Beernik, and M.E. Givens, *IEEE J. Quantum Electron*, **28** (1992) 1983.

[26] G. Zhang, and A. Ovtchinnikov, *Appl. Phys. Lett.*, **62** (1993) 1644.

[27] J. E. Geusic, W. B. Bridges and J. I. Pankove, *Proc. IEEE* **58** (1970) 1419.

[28] David Wood, *Optoelectronic Semiconductor Devices*, Prentice Hall, 1994.

[29] H. Kressel and M. Ettenberg, *J. Appl. Phys.* **47** (1976) 3533.

[30] H. Kressel et al., *Semiconductor Devices for Optical Communication*, Springer Verlag, 1980.

[31] M. B. Panish, I. Hayashi and S. Sumski, *Appl. Phys. Lett.* **16** (1970) 326.

[32] A. G. Milnes and D. L. Feucht, *Heterojunctions and Metal-Semiconductor Junctions*, Academic Press, 1972.

[33] *Private communication*, 2000.

[34] J. Minch, S. H. Park, T. Keating, and S. L. Chuang, *IEEE J. Quantum electron.*, **5** (1999) 771.

[35] S. Seki, T. Yamanaka, W. Lui, Y. Yoshikuni, and K. Yokoyama, *IEEE J. Quantum Electron.*, **30** (1994) 500.

[36] T. Ishikawa, T. Higashi, T. Uchida, T Yamamoto, T. Fujii, H. Shoji, M. Kobayashi, and H. Soda, *IEEE Photon. Technol. lett.*, **10** (1998) 1703.

[37] M. Hetterich, M. Dawson, A. Y. Egorov, and H. Riechert, *Appl. Phys. Lett.*, **76** (2000) 1030.

[38] S.S. Vishnubhatla, B. Eyglunet and J. C. Woolley, *Can. J. Phys.* **47** (1969) 1661.

[39] G. P. Agraval and N. K. Dutta, *Long-wavelength semiconductor lasers* (New York: Van Nostrand Reinhold), 1986.

[40] C. G. Van de Walle and R. M. Martin , *Phys. Rev. B* **35** (1987) 8154.

[41] R. S. Bauer and G. Margaritondo, *Phys. Today*, **40** (1987) 27.

[42] A. Baldereschi, S. Baroni and R. Resta, *Phys. Rev. Lett.*, **61** (1988) 734.

[43] C. G. Van de Walle, *Phys. Rev. B*, **39** (1989) 1871.

[44] S. L. Chuang, *Physics of Optoelectronic Devices*, New York : Wiley 1995.

[45] W. A. Harrison, J. Vac. *Sci. Technol.*, **14** (1977) 1016.

[46] J. Minch, S. H. Park, T. Keating, and S. L. Chuang, *IEEE J. Quantum electron.*, **35** (1999) 5.

[47] W. Shan, W. Waluekiewicz et al., *Phys. Rev. Lett.* **86** (1999) 1221.

[48] K. M. Yu, W. Waluekiewicz, W. Shan, et al., *Phys. Rev. B*, **61** (2000) R13337.

[49] W. Shan, W. Waluekiewicz et al., *J. Appl. Phys.* **86** (1999) 2349.

[50] W. Shan, W. Waluekiewicz et al., *Appl. Phys. Lett.*, **76** (2000) 3251.

[51] K. M. Yu, W. Waluekiewicz, W. Shan, et al., *Appl. Phys. Lett*, **78** (2001) 1017.

[52] I. Suemune, K. Uesugi and W. Waluekiewicz, *Appl. Phys. Lett.*, **77** (2000) 3021.

[53] J. D. Perkins et al., *Phys. Rev. Lett.*, **82** (1999) 3312.

[54] J. Hedder, S. W. Koch, J. L. Moleney and E. P. O'Reilly, *Appl. Phys. Lett.*, **77** (2000) 630.

[55] E. D. Jones et al., *Phys. Rev. B*, **60** (1999) 4430.

[56] E. D. Jones et al., *Proc. SPIE*, **52** (1999) 3621.

[57] A. Lindsay and E. P. O'Reilly, *Solid State Commun.*, **112** (1999) 443.

[58] T. Mattila, S.H. Wei and A. Zunger, *Phys. Rev. B*, **60** (1999) R11245.

[59] J. D. Perkins , A. Mascarenhas, Y. Zhang, J. F. Geisz, D. J. Friedman, J.M. Olson and S.R. Kurtz, *Phys. Rev. Lett.* **82** (1999) 3312.

[60] T. Ishikawa and J.E. Bowers , *IEEE J Quantum Electron.* **30** (1994) 562.

[61] S. J. Sweeny et al., *Phys. Stat. Sol.B* **223** (2001) 573.

[62] A. F. Phillips, S. J. Sweeny, A.R. Adams and P. J. A. Thijs, *IEEE J. Sel. Top. Quantum Electronics* **5** (1999) 401.

[63] S. Seki, H. Oohashi, H. Sugiura, T. Hirono and K. Yokoyama, *IEEE J. Quantum Electron.*, **32** (1996) 1478.

[64] T. R. Chen, B. Chang, L.C. Chiu, K. L. Yu, S. Margalit and A. Yariv, *Appl. Phys. Lett.*, **43** (1983) 217.

[65] R.F. Kazarinov and G. L. Belenky , *IEEE J. Quantum Electron.* **31** (1995) 423.

[66] J. W. Pan and J. I. Chyi , *IEEE J. Quantum Electron.* **32** (1996) 2133.

[67] F. Höhnsdorf, J. Koch, S. Leu, W. Stolz, B. Borchert and M. Druminski, *Electron. Lett.* **35** (1999) 571.

[68] K. Nakahara, M. Kondow, T. Kitatani, M. C. Larson and K. Uomi, *IEEE Photon. Technol. Lett.* **10** (1998) 487.

[69] S. Sato and S. Satoh , *Electron. Lett.* **35** (1999) 1251.

[70] I. A. Buyanowa, W. M. Chen and B. Monemar, *MRS Internet J. Nitride Semicond. Res.* **6** (2001)2.

[71] J. C. L. Yong , J. M. Rorison and I. White, *IEEE J. Quantum Electron.* **38** (2002) 1553.

[72] G. Lin and C. P. Lee , *Optical and Quantum Electronics* **34** (2002) 1191.

[73] P. Perlin, S. G. Subramanya , D. E. Mars, J. Kruger , N. Shapiro, H. Siegle, E. R. Weber, *Appl. Phys. Lett.* **73** (1998) 3703.

[74] M. Kondow, K. Uomi , A. Niva, T. Kitatani, S. Watahiki, and Y. Yazawa, *Jpn. J. Appl. Phys. Lett.* **73** (1998) 3703.

[75] C. Elmers, F. Hohnsdorf, J. Koch, C. Agert, S. Leu, D. Karaiskaj, M. Hofmann *Appl. Phys. Lett.* **74** (1999) 2271.

[76] H. P. Xin, C. W. Tu, *Appl. Phys. Lett.* **72** (1998) 2442.

[77] T. L. Koch, U. Koren, R. P. Gnall, C. A. Burrus and B. I. Miller , *Electron. Lett.* **26** (1988) 1431.

[78] J. W. Matthews and A. E. Blakeslee , *J. Cryst. Growth* **24** (1974) 188.

[79] A. Ghiti and U. Ekenberg, *Semicond. Sci. Technol.* **9** (1994) 1575.

[80] B. I. Miller, U. Koren, M. G. Young and M. D. Chieh, *Appl. Phys. Lett.* **58** (1991) 1952.

[81] I. Vurgaftman, J. R. Meyer, and L. R. Ram –Mohan, *J. Appl. Phys.* **89** (2001) 5815.

[82] C. Silfvenius, B. Stalnacke and G. Landgren , *J. Cryst. Growth* **170** (1997)122.

PUBLICATIONS

1. B. GÖNÜL, O. ÖZER, B. GÖNÜL and F. ÜZGÜN, Exact Solutions Of Effective-Mass Schrödinger Equations, Modern Phys. Lett. **A 17** (2002) 2453.

2. B. GÖNÜL, F. KOÇAK, H. TOKTAMIŞ, M. ODUNCUOĞLU, A, Theoretical Comparison Of the Band-Offset Ratios Of Phosphorus-Aluminium-and Nitrogen Based 1.3 μm QW Lasers, Submitted to Physica E (June 2003).